Authors answers to tc-2020-354 comments

May 6th, 2021

Dear Editor,

We are pleased to submit the revised manuscript of our paper entitled "A generalized stress correction scheme for the MEB rheology: impact on the fracture angles and deformations" by Mathieu Plante and L. Bruno Tremblay.

We would like to thank the reviewers for their useful comments and suggestions. We have modified our manuscript according to most suggestions of the reviewers. This helped improve the clarity of the article substantially.

Thank you for your consideration for publication.

Sincerely,

On behalf of all the authors,
Mathieu Plante

Note:

- The referee comments are shown in black,
- The authors answers are shown in blue,
- *Quoted texts from the revised manuscript are shown in italic and in dark blue.*
- Amendments made to the responses in the open discussion are shown in green

Answers to tc-2020-354 RC1

June 21st, 2020

Note:

- The referee comments are shown in black,
- The authors answers are shown in blue,
- *Quoted texts from the revised manuscript are shown in italic and in dark blue.*
- Amendments made to the responses in the open discussion are shown in green

Review of "A generalized stress correction scheme for the MEB rheology: impact on the fracture angles and deformations" by Plante and Tremblay (tc-2020-354).

This manuscript is a generally well written and easy to follow description of an extension to the MEB model of Plante et al (2020), but also has implications for other MEB implementations. This extension addresses two problems of the original model: large (numerical) error growth, which may be model code specific) and too large fracture angles (which is probably not model-code specific. The new scheme allows to specify a more general correction of stress states that exceed the Mohr-Coulomb failure criterion. Sensitivity experiments in uniaxial compression illustrate that the parameterization indeed reduces the error growth and also reduces the fracture angles towards more realistic values. From the sensitivity experiments a preferred parameter set is determined. This is a very useful addition to the development of MEB rheology (and code) and should be published subject to minor revisions.

We thank the referee for his or her thorough review of the manuscript and constructive comments.

My main point of critique is that the manuscript is missing a bit of general introduction and a clear problem statement. To my mind, the manuscript can be improved by taking the reader more by the hand than is done. This only requires a few sentences here and there or maybe an additional paragraph, e.g.

(1) what do we expect from a "brittle" model in contrast to a "granular material". The concept of "granular material/flow" is used often in the text, but it is not clear (from the text) how the brittle part of the model relates to that. Do we expect that a brittle model represents a granular material properly?

Brittle and ductile are types of fractures: a brittle fracture occurs with little prior plastic (permanent) deformation, and ductile fracture occurs after significant plastic deformations. A granular material, on the other hand, is a type of material: i.e., a composite of aggregated

granules, as opposed to metals or crystals). Granular theories describe the fractures and deformations of granular materials in terms of the distribution of contact normal between individual grains.

A brittle model is thus expected to represent the nucleation and propagation of cracks in a material, effectively producing a material discontinuity in the material properties. A granular model typically uses a Mohr-Coulomb yield curve and granular flow rules (sliding along fracture planes with more or less dilatation) to govern the material dynamics.

In the MEB model for instance, the damage parameterization corresponds to the "brittle" behaviour of sea ice, and the granular behaviour is reflected in the choice of a Mohr-Coulomb yield curve.

This is now clarified in a new paragraph at the beginning of the model section 2.2, L116-120 and in section 4.3.3.

(2) state the issues with sea models and MEB in particular that are addressed in this paper in separate paragraphs. Now the angle-issue is mentioned in the middle of a paragraph that is introduced by: "The damage parameterization is relatively new, …"

>> We re-wrote the introduction (as suggested) to better introduce these issues, as well as addressing the previous and following comments from the reviewer. We address the challenges in representing the fracture of sea ice in the context of large-scale sea-ice models that are based on the continuum assumption, and then address issues that are more specific about the MEB rheology.

(3) discuss if the new scheme can be also useful for other implementations of MEB (e.g. neXtSim)

>> Yes, the new scheme can be used in other implementation of the MEB model (e.g. neXtSIM). Specifically, our implementation represents a generalization of the damage parameterization that can be easily implemented numerically and used to improve the performance of MEB models. Our results also show that the new scheme can be used to tune the simulated fractures closer to observations. These statements are added in the discussion section, L398-406 and in conclusions.

There are some technical issues (figure referencing and captions) detailed below.
The points below sometimes repeat my main points.

page 1

Abstract: General background and (more importantly) a clear problem statement is missing from the abstract. E.g., the problem of too large angles is not stated and the error growth is also only mentioned as the target of the new parameterization. It would help to have more context here already (1-2 extra sentences).

>> A clearer statement for the motivation of this study in included in the revised manuscript. The

abstract now reads:

"The Maxwell Elasto-Brittle (MEB) rheology uses a damage parameterization to represent the brittle fracture of sea ice without involving plastic laws to constrain the sea-ice deformations. The MEB damage parameterization is based on a correction of super-critical stresses that binds the simulated stress to the yield criterion but leads to a growth of errors in the stress field. A generalized damage parameterization is developed to reduce this error growth and to investigate the influence of the super-critical stress correction scheme on the simulated sea-ice fractures, deformations and orientation of Linear Kinematic Features (LKFs). A decohesive stress tensor is used to correct the super-critical stresses towards different points on the yield curve. The sensitivity of the simulated sea-ice fractures and deformations to the decohesive stress tensor is investigated in uniaxial compression experiments. Results show that the decohesive stress tensor influences the growth of residual errors associated with the correction of super-critical stresses, the orientation of the lines of fracture and the short-term deformation associated with the damage, but does not influence the long-term post-fracture sea-ice deformations. We show that when ice fractures, divergence first occurs while the elastic response is dominant, and convergence develops post-fracture in the longer-term when the viscous response dominates -- contrary to laboratory experiment of granular flow and satellite imagery in the Arctic. The post-fracture deformations are shown to be dissociated from the fracture process itself, an important difference with classical Viscous Plastic (VP) models in which large deformations are governed by associative plastic laws. Using the generalized damage parameterization together with a stress correction path normal to the yield curve reduces the growth of errors sufficiently for the production of longer-term simulations, with the added benefit of bringing the simulated LKF angles closer to observations (from $40-50^\circ$ to $35-45^\circ$, compared to $20-30^\circ$ in observations)."

l3: any correction path: unclear "any"

>> This was replaced by "*towards different points on the yield curve*" in the revised manuscript.

l18: significantly: repetition

>> Corrected as suggested by the reviewer.

l22: the presence of and deformations along LKFs

>> Corrected as suggested by the reviewer.

l30: Hunke, 2001: not sure if this is an appropriate reference (for what)?

>> We removed this reference in the revised manuscript.

l44: "The fracture angle simulated by the MEB and standard VP models" It will be easier to follow, if you dedicate a separate paragraph (or at least an introductory sentence to this paragraph) to the fracture angles as a problem statement before describing what VP and MEB models do wrong.

>> We agree with the reviewer. We revised the introduction and added a new paragraph that focuses on the representation of fracture angles in both the VP and MEB models.

ll60 I think that the problem statement is not clear enough. Unless you are very familiar with the details of the implementation of MEB models, it's not clear where Plante et al (2020) had numerical difficulties and if this is specific to their implementation. It should be clear if this will also be of value for, e.g. neXtSIM, or Dansereau et al.

Also the fracture angle problem is somewhat buried in the introduction and should be more prominent, because the paper devotes a large part to this.

>> We now devote a paragraph on the MEB model behaviour where these points are clarified as suggested. We specify that the numerical difficulty is related to the integration of the residual errors in the damage parameter, and is associated with the damage equation used in all MEB models.

l62: (Sulsky and Peterson, 2011) fix parentheses

>> Corrected as suggested by the reviewer.

l81: (Plante et al., 2020) fix parentheses

>> Corrected as suggested by the reviewer.

l96: is -> in

>> Corrected as suggested by the reviewer.

l104: "resulting in dominant elastic component"? not clear, something missing?

>> This refers to the dominance of the elastic term vs. the negligible viscous term in the constitutive equation. We clarified these lines in the revised manuscript, which now read:

"[…] the elastic term dominates when the ice is undamaged while the viscous term dominates when the ice is heavily fractured."

ll117: maybe put \mu, \phi, c into Fig1 for better illustration?

>> We added the parameters as suggested by the reviewer.

eq 16: where does the "some algebra" start from? Maybe add a little more explanation here to guide the reader.

>> We added more information in the revised manuscript. Eq. 19 (in the revised manuscript) is found by finding the intersection point between the yield curve (Eq. 10) and the line

corresponding to the stress correction. We add the mathematical expression of the stress correction line, such that the algebra is more straightforward.

l148: “something that is not possible in the standard parameterization otherwise \Psi …” please rephrase.

>> This sentence is clarified in the revised manuscript, and now reads:

“[…] as opposed to the standard parameterization in which case any super-critical stress is returned to the origin.”

l166: on -> of

>> Corrected as suggested by the reviewer.

l208: asymmetry factor: not immediately clear why this measures error. I assume that you expect perfectly symmetric solutions about the center line, but I think that this needs to be explained.

>> This diagnostic is explained in more details in section 4.3.1, L274-L285 in the revised manuscript, including its definition about the center line. We specify that it measures the cumulated far-field response to all residual errors produced from the start of the simulation. As opposed to the amplification factor R, which only measures the maximum local amplification of the residual error by the damage parameterization, the asymmetry measures the cumulative and longer-term effect of the residual errors on the model solution.

The same is true for “damage activity”, what do you want to use this for and how does this diagnostic achieve that.

>> The damage activity is only used to indicate the onset of fracturing and the short time scale associated with the development of fracture. It serves to show that the onset of the growth of errors in the solution is associated with the fracture. This is specified in section 4.3.2, L290-292 in the revised manuscript.

eq.26/27. the notation is a bit unusual and looks a little like (pseudo-) code. Why not use standard indexing as one would expect in a maths text?, e.g. \left(\sigma_{II}\right)_{n_x-i,j}

>> We agree and the format is corrected in the revised manuscript.

l235: 0.29 N/m? units?

>> This is an error and is corrected to N m^{-2}.

l243: “mostly elastic with divergence along the fracture line” Where do we see that divergence? In Fig3 I mostly see negative divergence = convergence.

>> This is illustrated in Fig. 4b (the reference is added in the revised manuscript). Figure 3 shows the deformations after 2 hours of simulations, in which points the deformations are dominated by the post-fracture (viscous) convergence. This is also clarified at the beginning of this paragraph, at L322-324 in the revised manuscript.

l248/9 The references to figure 4 are not correct. There is no Fig 4i, then it's not clear from the caption, what we are seeing in color (damage?). It would help to add the timing in the plot (maybe top right or bottom left of rhs column).

>> There were errors in the labelling. This is corrected in the revised manuscript. We also improved the labels and captions in this figure.

l251: here and everywhere else: Units should NOT be in italics).

>> Corrected as suggested by the reviewer.

l254: 10−6 Nm−2 (unit not in italics): in 4.1 it was 1e-8!! In Fig5 it seems to be 1e-8 as well.

>> It should indeed indicate 10-8, this is corrected in the revised manuscript.

l254:are -> is

>> Corrected as suggested by the reviewer.

l254: "damage error amplification ratio R" maybe refer to equation 23 here?

>> We agree and added the reference in the revised manuscript.

l258: indicate -> indicates

>> Corrected as suggested by the reviewer.

In Figure 6 the panels for eps_asym and R_max are exchanged wrt to Figure 5. Why confuse the reader?

>> We agree with the reviewer and interchanged the panels in the revised manuscript.

l263: "the production of" could be removed

>> Corrected as suggested by the reviewer.

l264: I would argue for \gamma \ge 0 the improvement is significant (including 0). But the asymmetry also grows for \gamma > 0 and only for values > 45 it seem to stay low. Why not discuss that here?

>> We added a few lines in the revised manuscript in section 5.2, L341-350 to address this comment, instead of only bringing this point in the discussion section. We note that the improvement by the generalized parametrization is limited by the fact that the damage remains an integrated parameter, and that the residual error remains very influential in heavily damaged ice due to by the non-linear relationship between the sea ice deformation and the damage. We specify that the main improvement here is the removal of the spikes in the amplification ratio. We also note that the slower growth of asymmetries in the case of large correction angles are partly attributed to the slower development of the discontinuity. Thus, as we increase gamma, the improvement comes increasingly at the cost of losing the brittle behaviour of sea ice.

l286: "Based on these results, we suggest the use of a correction path that is normal to the yield criterion (\gamma = arctan \mu, see black points in Fig. 9)." my say, \gamma = \phi in this case, (isn't it)?

>> It is not the case. \gamma and \mu are defined in the stress invariant space, whereas the friction angle \phi is defined in the Mohr stress space. That is, the angle of friction \phi does not correspond to the angle spanned from the x axis to the yield curve in the stress invariant space. Rather, the slope of the yield curve in the stress invariant space is \mu = sin(\phi). Thus, writing \gamma as a function of \phi would yield: \gamma = arctan(sin(\phi)).

l331: "are robust to the exact" -> are not sensitive to the exact, are robust with respect to the exact …

>> Corrected as suggested by the reviewer.

l335: reach -> reaches

>> Corrected as suggested by the reviewer.

l335: elastic wave are however no-longer -> elastic waves, however, are no longer …

>> Corrected as suggested by the reviewer.

l344: in -> is

>> Corrected as suggested by the reviewer.

l349: the uniaxial -> a uniaxial

>> Corrected as suggested by the reviewer.

l351: not sure if "post-fracture" (or pre-fracture) is grammatically correct. I would use "after (and before) fracture" in most places in this manuscript

>> We prefer to keep "post-fracture" as it is concise and often used in the field to describe material behaviour.

l352: “contrary to laboratory experiments of granular materials and satellite observations of sea ice.” A short discussion about to what extent we expect granular behavior in an MEB model seems in place (not here in the conclusions but somewhere in the introduction?), in order to understand if this is an encouraging or a discouraging result

>> We agree with the reviewer and provide more background on the fracture angles and dilatancy in section 4.3.3. This section (4.3.3) and section 4.1 in the revised manuscript are re-written to clarify the granular character of sea ice and how it is related to fracture angles in uniaxial compression tests.

l361: “the production of” remove, see above

>> Corrected as suggested by the reviewer.

Figure3: mixiumum -> maximum/minimum?

>> This is corrected to “maximum” in the revised manuscript.

Figure 4. What are the meaning and the units of the color scale? Is this for the control simulation only?

>> This figure is for the control run and the color indicates the local damage (unitless) of each scatter points. These precisions are added in the revised manuscript.

Fig9: “The theoretical fracture angle from the Mohr-Coulomb and Roscoe theories are indicated by dashed and dash-dotted lines for reference.” something like this, could also be useful in Fig7.

>> We agree and added these precisions in the captions of both Fig 7 and 9

Answers to tc-2020-354 RC2

June 21st, 2020

Note:

- The referee comments are shown in black,
- The authors answers are shown in blue,
- *Quoted texts from the revised manuscript are shown in italic and in dark blue.*
- Amendments made to the responses in the open discussion are shown in green

Referee's Report on: A generalized stress correction scheme for the MEB rheology: impact on the fracture angles and deformations by Mathieu Plante and L. Bruno Tremblay

This manuscript describes a modification of the return algorithm for supercritical stresses in the Maxwell-Elasto-Brittle (MEB) model for sea ice. The stated purpose of this modification is to better match simulated and observed fracture angles, and to reduce numerical growth of errors over the course of the simulation. The modification is tested on uniaxial deformation of a rectangular patch of sea ice. The modifications provide improvement over the previous approach but do not yet quite match observation. Overall, the goal and methods are clearly stated, although some notation is sloppy.

>> We thank the referee for his or her thorough review of the manuscript and constructive comments.

Trying to adjust the return algorithm to influence the failure angle is rather an indirect course of action. There does not appear to be a direct prediction of failure angle, just a demonstration through a full numerical simulation. It would be good to emphasize/clarify this point in the text (if it is in fact true), or explain how to predict the failure angle (if it is not true).

>> It is correct that we do not use the return algorithm to prescribe the fracture angle. The original goal of the study was to reduce the integration errors in the MEB rheology and study the sensitivity of the model to the return algorithm, given that the exact path along which the super-critical stresses should be returned to the yield curve is not known a priori. The fact that the fracture angle is in better agreement with observations when we use an algorithm that minimizes

the error growth is a by-product of this original goal. This is clarified in the abstract at L5-7, L17-18, in the introduction at L86-88 and in the discussion in the revised manuscript.

A more direct approach to prescribe the fracture angle would be to introduce a decohesive strain when damage increases, in the manner similar to the fracture algorithm of Schreyer et al. (2006), or Sulski and Peterson (2011). This was not included in the present parameterisation, as it would represent a significant modification of the MEB rheology, but will be considered for future model developments. These precisions added in a paragraph that we add at L214-219 in the revised manuscript.

One aspect that is lacking in the presentation is the behavior of the numerical algorithm when the mesh size is changed. Fracture models are notorious for illposedness and it would be good to illustrate that this model's predictions do not depend on the mesh size. It is also common for the failure angle to depend on the mesh aspect ratio. Both mesh refinement and aspect ratio need to be explored.

>> A more complete study of the sensitivity of the model to spatial resolution is the subject of another paper in preparation (to be submitted in the Fall). Preliminary results using a simple shear flow in a 1D channel show that the "boundary layer", or spatial scale l where damage occurs decreases when the spatial resolution is increased, while the number of grid points required to resolve the "boundary layer" increases. This opens the door to a series of new questions that we prefer to keep in a separate paper.

In the context of this study, we did simple uniaxial loading experiments with different spatial resolution and sample aspect ratio. We find that the simulated angle of fracture, the growth of numerical errors and the dependency of the fracture angle on the correction path are robust to the exact choice of model resolution and to the ice sample aspect ratio. This is now included in the discussion in the revised manuscript by broadening the scope of its last paragraph, previously dedicated to heterogeneity (L430-441).

We did not test the sensitivity of the results to the mesh aspect ratio. This would require significant modifications to the McGill Sea Ice Model. The code is also written using a Cartesian coordinate system and it is customary to keep dx equal to dy in such models.

I have some additional questions, comments, and suggested improvements.

1. Abstract: The VP model does not include fracture.

>> We rephrased the problematic sentence in the abstract from: "*The post-fracture deformations are shown to be dissociated from the fracture process itself, an important difference with classical Viscous Plastic (VP) models.", to:*

"The post-fracture viscous deformations in the MEB model are shown to be dissociated from the fracture process itself, an important difference with classical Viscous Plastic (VP) models in which large deformations are governed by associative plastic laws".

We also note that while the VP models do not resolve brittle fractures and the LKFs are not pre-conditioned by discontinuities in material properties, they do represent ductile fractures with simultaneous deformations that are determined by the yield stress as governed by plastic laws.

2. Page 3: You are using an Eulerian grid but I don't see equations that show advection of parameters (eg damage parameters). Are you assuming small deformations only? (See equation 12, for example.)

>> We do advect the ice thickness and concentration parameters, but neglect the advection of damage, given that the fracture process occurs in a timescale (seconds) much shorter that the advection timescale (hours). The advection of damage should be included in longer-term integration of the MEB model. Adding the advection of damage does not change the results and conclusions presented in this paper but it increases the localisation of the ice fractures. This results in higher damage values that in turn increases the rate of ridging. This has been clarified in section 2.4, L165-169 in the revised manuscript.

3. Page 4: Equation 5. Is a superposed dot the same as a partial time derivative or a material time derivative? Is this rate equation objective? Is ice deformation really rate dependent? Are there experiments about that?

>> The superposed dot is a partial time derivative. In the case of damaged ice, the large-scale sea ice deformations (especially ridging) are traditionally seen as "plastic" (see Coon et al. 1974), with stresses that are strain-rates independent that are rate-independence, in accord with laboratory experiments (Tuhkuri and Lensu, 2002). The post-fracture viscous deformations are not in accord with field observations and rather represent a simplification of the larger-scale plastic regime. These points are clarified at L142-L143 of the revised manuscript.

4. Page 4: Equations 6 and 7: You are using multiple notations for the same thing: x and y components, 1 and 2 components. In Eq. 5, C is a fourth order tenor, Eq. 6 is a 2 × 2 matrix (components of a second order tensor?).

>> We changed the indices "1" and "2" for "x" and "y" in Eq. 7, in the revised manuscript, as suggested by the reviewer.

As the reviewer points out, the tensors defined in Eq. 5 are presented in Eq. 6 and 7 using a matrix notation. This notation is often used in the literature to concisely write the components of the elastic tensor, based on the symmetry of the stress and strain tensors. It is obtained by laying out the 3 (in 2D) independent components of the 2nd order stress and strain tensors into a single row, such that the components of the 4th order tensor C are written in a 3x3 matrix (6x6 in 3D). See Rice (2010) for reference. This is clarified at L126-128 of the revised manuscript.

5. Page 5: Probably helpful to define σI and σII in terms of stress components.

>> This is added as Eq. 11-12 in the revised manuscript, as suggested by the reviewer.

6. Page 6: Line 150: What is the 'standard' path?

>> The “standard” path refers to the original return algorithm in the EB and MEB damage parameterization (Rampal et al. 2016, Dansereau et al. 2016), where the super-critical stresses are relaxed along a line that runs through the origin. This is now specified in a new paragraph added at the end of section 2.4 in the revised manuscript.

7. Page 6: Line 151: Change ’to for’ to ’for’.

>> Corrected as suggested by the reviewer.

8. Page 6: Line 162: Schreyer et al do not use ’granular theory’, assuming that means models of granular flow. It is also confusing to refer to σc as a decohesive stress tensor since it has no apparent connection to Schreyer et al.

>> We remove “granular theory” in this sentence and use the term more carefully throughout the revised manuscript. We also clarified our references to Schreyer et al. (2006).

Although our work is inspired by Schreyer et al. 2006, the name “decohesive stress tensor “ is not a direct reference to their algorithm, but rather a reference to the fact that this stress is produced in association with the development of damage, hence to the decohesion of the ice material. We nonetheless note that our mention of Schreyer et al. 2006 refers to their use of a decohesive strain that is subtracted from the local elastic strain in the stress-strain relationship when the ice fractures, effectively relaxing the stress rates. This was clarified in the revised manuscript at L214-219, which now reads:

“Note that the decohesive stress tensor used in this parameterization has a similar role as the decohesive strain used in the Elastic-Decohesive model (Schreyer et al., 2006). In Schreyer et al (2006), the decohesive strain represents the discontinuity in sea-ice displacement associated with a fracture and relaxes the effective stress rates. It is derived from a decohesion function that depends on the mode of failure. Here, we do not define the strain discontinuity associated with the fractures, but use the decohesive stress tensor $\boldsymbol{\sigma}_D$ to prescribe the orientation at which the stress state is relaxed back onto the yield curve. This only indirectly influences the local strain rate via the constitutive equation.”

9. Page 7: Line 177: Change ’correspond’ to ’corresponding’.

>> Corrected as suggested by the reviewer.

10. Page 7: last line: What is included in the ’solution vector’?

>> The discretized set of equation corresponds to a system of N non-linear equations in the form of :

$$\mathbf{A}\,\mathbf{x} = \mathbf{b}\,,$$

where **x** is a vector formed by stacking all the $u_{i,j}$ components followed by the $v_{i,j}$ components, A is a NxN matrix with components that contains coefficients for the $u_{i,j}$ and $v_{i,j}$ dependent terms and B is a vector of length N containing the other terms. Then, the solution vector **F** is written as:

$$\mathbf{F} = \mathbf{A}\,\mathbf{x} - \mathbf{B}\,.$$

We chose not to include these details in the revised manuscript, as it would necessitate a lengthy numerical description, and added instead a reference to Lemieux et al., (2014) for readers in search of these precisions.

11. Page 8: Line 204: τa is a vector. I assume the scalar value you assign to it is for one component and the other is zero. (Also Page 9, Line 245.)

>> Yes. This precision is added at L256 in the revised manuscript.

12. Page 9: First line: Please give a reference showing the connection between failure in granular material and sea ice under uniaxial compression.

>> This section (4.3.3) and section 4.1 are re-written in the revised manuscript to clarify the granular character of sea ice and how it is related to fracture angles in uniaxial compression tests. A few references are added, such as Bardet et al. (1991) for granular geo-materials in uniaxial compression, Wachter et al. (2008) for fracture angles in ice samples, Overland et al (1998) for shear bands observations in the Arctic.

13. Page 9: Line 226: I don't see a definition of δ.

>> It is defined above Eq. 29, as the angle of dilatancy.

14. Page 9: Line 228: 'In general, the fracture angle ...' is this the fracture angle for sea ice?

>> We changed "In general" for "In most materials"

15. Page 9: Line 244: Change 'waves' to 'wave'.

>> Corrected as suggested by the reviewer.

16. Page 9: Line 248: '4 cfi)' means Figure 4?

>> This was an error in the labeling, and is corrected in the revised manuscript

17. Page 10: Line 254: Change 'are' to 'is'. I do not see in Fig. 5 that large values of R is associated with growth in εsym. Can you illustrate this better?

>> We do not expect a correlation between R, the largest local error in the damage factor Psi, and ε_{sym}, which represents the domain-integrated asymmetries in the stress field. Specifically, ε_{sym} corresponds to the cumulated the far-field response to all residual errors of previous time iterates. It grows with the onset of fracture (with large R values), given that the damage parameterization is the largest source of errors. With time, however, the far-field response to previous errors become large and dominates over the new errors in the damage factor Psi. We clarified this point and these variables in section 4.3.1 and at L281-L285 in the revised manuscript.

18. Page 10: Line 255: Change 'growths R' to 'growth in R'.

>> For consistency, we changed for "error amplification ratio R", as used throughout the manuscript.

19. Page 10: Line 258: Change 'indicate' to 'indicates'.

>> Corrected as suggested by the reviewer.

20. Page 10: Line 269: Change 'depends on corrected' to 'depend on the corrected'.

>> Corrected as suggested by the reviewer.

21. Page 10: Lines 274-278: MEB and VP (and granular material models) make different predictions. Is there any evidence for your model behavior in experiments? The VP model is based on plasticity there is no fracture, so no 'post-fracture behavior.'

>> As discussed in comment #3 above, the large-scale sea-ice deformations are mostly "plastic" (see Coon et al., 1974, Tuhkuri and Lensu, 2002). The post-fracture viscous deformations in the MEB model thus do not correspond to field observations and represent a simplification of the plastic regime. The VP model simulates the plastic deformations associated with the ductile fractures, which corresponds to the observed material behaviour at the macro-scale. The VP model however does not represent the brittle component of the fractures or discontinuities in material properties, which occur at the smaller scales but may influence the fractures orientation and other deformation statistics. These points are clarified at L363-L366 in the revised manuscript.

22. Page 11: Line 284: Change 'approaches' to 'approach'.

>> Corrected as suggested by the reviewer.

23. Page 11: Line 286: Change 'sensitive other' to 'sensitive to other'.

>> Corrected as suggested by the reviewer.

24. Page 11: Line 290: Change 'increase' to 'increases'.

>> Corrected as suggested by the reviewer.

25. Page 12: Line 332: Change ’divergence’ to ’divergent’.

>> Corrected as suggested by the reviewer.

26. Page 12: Line 335: Change ’reach’ to ’reaches’. Change ’wave’ to ’waves’.

>> Corrected as suggested by the reviewer.

27. Page 13: Line 357: Change ’generalizes’ to ’generalized’.

>> Corrected as suggested by the reviewer.

References:

Bardet, J.: Orientation of shear bands in frictional soils, Journal of Engineering Mechanics - ASCE, 117, 1466–1484, https://doi.org/10.1061/(ASCE)0733-9399(1991)117:7(1466), 1991.

Coon, M. D., G. A. Maykut, R. S. Pritchard, D. A. Rothrock, and A. S. Thorndike. 1974. Modeling the pack ice as an elastic-plastic material. AIDJEX Bulletin, 24, H05.

Dansereau, V., Weiss, J., Saramito, P., and Lattes, P.: A Maxwell elasto-brittle rheology for sea ice modelling, The Cryosphere, 10, 1339–
1359, https://doi.org/10.5194/tc-10-1339-2016, 2016.

Lemieux, J.-f., Knoll, D. A., Losch, M., and Girard, C.: A second-order accurate in time IMplicit – EXplicit (IMEX) integration scheme for sea ice dynamics, Journal of Computational Physics, 263, 375–392, https://doi.org/10.1016/j.jcp.2014.01.010, 2014.

Overland, J. E., McNutt, S. L., Salo, S., Groves, J., and Li, S.: Arctic sea ice as a granular plastic, J. Geophys. Res., 103, 21845–21868, 1998.

Rice, J. R,: Solid Mechanics, Harvard University, 2010.

Schreyer, H. L., Sulsky, D. L., Munday, L. B., Coon, M. D., and Kwok, R.: Elastic-decohesive constitutive model for sea ice, Journal of Geophysical Research: Oceans, 111, C11S26, https://doi.org/10.1029/2005JC003334, 2006.

Sulsky, D. and Peterson, K.: Toward a new elastic – decohesive model of Arctic sea ice, Physica D Nonlinear Phenomena, 240, 1674–1683, https://doi.org/10.1016/j.physd.2011.07.005, 2011.

Tuhkuri, J., and Lensu, M., Laboratory tests on ridging and rafting of ice sheets, *J. Geophys. Res.*, 107(C9), 3125, doi:10.1029/2001JC000848, 2002.

Wachter, L. M., Renshaw, C. E., & Schulson, E. M. (2009). Transition in brittle failure mode in ice under low confinement. *Acta Materialia*, **57**(2), 345-355.

Answers to tc-2020-354 RC3

June 21st, 2020

Note:

- The referee comments are shown in black,
- The authors answers are shown in blue,
- *Quoted texts from the revised manuscript are shown in italic and in dark blue.*
- Amendments made to the responses in the open discussion are shown in green

In this paper the authors introduce a modification of the MEB rheology in the form of a generalized damage parameterisation. They then proceed to test this new parameterisation using an idealised uniaxial loading setup. They find that the new parameterisation influences the resulting fracture angle, bringing it in the range of observations. The paper is well written and clear, using good English and sentence structure, and a logical flow from section to section and paragraph to paragraph.

The introduction of a modification of the MEB rheology is a niche topic, but potentially an important one and certainly one relevant for publication in the Cryosphere. As it stands, the paper has some faults I would like the authors to address. I expect they can do this adequately and that the resulting work will be fit for publication in the Cryosphere.

We thank the referee for his or her thorough review of the manuscript and constructive comments.

Major comments:

It is not clear why the authors are proposing this addition to the MEB. Is it numerics or physics, or something else? You say something general at the start, but it's vague and really only says what your modification does, not why you want to do it in the first place. This point should be crystal clear and guide the entire paper. Ideally the authors should say something like: "we want to introduce this scheme because we know it represents better the physics (and is incidentally better for the numerics). We see this by looking at the fracture angles (or some other measure)". Such a statement at the top would make this paper very strong.
An admittedly overly harsh evaluation of the current state is that the authors change something for dubious reasons and get a different response – so why should we care? Is this the right result, but for the wrong reasons? I don't think that's a fair assessment, but unless the motivation is clearer it will be the impression a critical reader gets.

>> We re-wrote the introduction to better state our objectives. The goal of the study is to reduce the integration errors in the MEB rheology and study the sensitivity of the model to the stress correction scheme, given that the exact path along which the super-critical stresses should be returned to the yield curve is not known a priori. This is clarified in the abstract, at L84-L90 and at L180-L188 in the revised manuscript.

We also add that our assessment of the sea ice deformations resulting from the use of a damage parameterization in the MEB model contributes to the current effort to assess the difference between different rheologies in reproducing satellite-derived sea-ice deformations (the FAMOS Sea-Ice Rheology Experiment (SIREx), https://epic.awi.de/id/eprint/48616/, with two papers currently under review in JGR). This is mentioned in the revised introduction.

Related to this lack of clear focus, I find it difficult to understand why you do
the experiments that you do, so reading sections 4 and 5 is more demanding of the reader than it need be.

>> There is a clear need to standardized simple idealized experiments to test/evaluate different rheological models. This was identified at the workshop "Defining a cutting-edge future for sea-ice modelling" (Laugarvatn, Iceland, 2019) and again recently at the online workshop Modeling the Granular Nature of Sea Ice (https://seaicemuri.org/workshop.html). In both workshops, the simple uni-axial loading test (used in Ringeisen et al. (2019, 2020) received good acceptance for the community. This choice of experiment is clarified in section 4.1 of the revised paper.

I also question the fact that the authors don't introduce heterogeneity into their model. They even point out themselves that it "is responsible for much of the brittle material behaviour in progressive damage models" and indicate that the residual errors are not important in a heterogeneous field – which is what MEB is supposed to give. This choice needs to be much better justified than is currently done.

>> We did not include heterogeneity in order to clearly identify the model performance (both numerics and physics). The issues related to the error growth leading to asymmetry in a problem with full symmetry and their impact on the fracture angles could not be addressed using heterogeneity. This was clarified in the revised manuscript at L258-261. We also clarify at L438-441 in the revised manuscript that the heterogeneity is responsible for the localisation and intermittency of sea ice, properties that are not investigated in our manuscript.

Finally, there's almost a hostile tone towards the MEB rheology in the discussion and conclusion section. The authors are practically gleeful in pointing out various faults of the model that are not relevant to the modifications they propose. It is of course fine to point out the faults of MEB - which apparently are plentiful – but the way it is done here borders on un-professional, in my opinion.

>> This is a serious accusation (unprofessionalism). We would ask that the reviewer identify the offending sentences and we will respond promptly whether the paper is accepted or not.

Clearly, this is not our point of view. We disagree that our tone is hostile towards the MEB

model. We developed the only (to our knowledge) implementation of this rheology in a finite difference framework in order to be able to study the difference in physics independent of the numerics (other MEB implementations are done in Finite Element). Our study of the numerical and mechanical behaviour of this rheology is in the prospect of better understanding how the damage parameter simulates the deformations and to identify the key elements that can be useful to other models as we aim for higher resolution products. The current paper is a follow-up to an earlier paper where those issues were raised but not addressed. Our goal is to improve sea ice modeling in general and we believe that a multi-model approach towards this goal is very useful.

Minor comments:

L16: The formulation makes it sound as if leads and LKFs are interchangeable, but they are not.

>> We agree and removed to mention to LKF in this sentence.

L120: Shouldn't the cohesion be a function of resolution (see Weiss, 2007)? If that's the case, how do you get the same value from large scale and the lab?

>> The material strength is a function of the resolution, and we do expect smaller values at the large scales (kms in our model) than in laboratory experiments, which usually find strengths that are one or more orders of magnitude larger than what we use in our study (10 kN m^{-2}). Our choice of cohesion is based on results from the ice bridge experiments of Plante et al. 2020, and coherent with what has been used in other studies using the MEB rheology (e.g. Dansereau et al. 2016, 2017, 2019, and also in Rampal et al. 2016, 2019).

L135: What's the physical justification for proposing this generalised stress correction?

>> As we mentioned above, we develop the generalised stress correction in part to improve the issues identified in our previous paper, and in part to assess the influence of the super-critical stress correction on the simulated fractures and deformation, with minimal chances to the damage parameterization. This is clarified in the revised manuscript at L84-90 and at the beginning of section 3.

Note that in the original parameterization, the choice of defining the damage parameter in terms of the amount of stress in excess of the yield curve was made to offer numerical robustness and simplicity. In a perfect model for instance, this overshoot would approach zero. A physically meaningful definition of the damage parameter could involve thermodynamics relations as the stress state approaches the yield curve (see for instance Murakami 2012), or use discrete cycling methods (as in the models of Main., 2000, Amitrano and Helmstetter., 2006, Carrier et al., 2015), but would represent a significant modification of the damage parameterization. This is considered for future model development but out of the scope of this paper.

L222: Mohr-Coulomb and Roscoe theories both concern granular materials, but hear we're dealing with the fracturing of a solid. Are they still valid? Please elaborate.

>> Sea ice is a granular material. Sea for instance books from Leppäranta (2011), Weiss (2013),

and the recent workshop “Modeling the Granular Nature of Sea Ice” (https://seaicemuri.org/workshop.html), bringing scientists from all around the world working on this topic, for reference.

L248: There’s a lot of information in figure 4 and the reader needs more help in deducing why you created it and what it’s supposed to tell us.

>> Additional information is included in the figure caption of the revised manuscript, which now reads:

“Scatter plots of local stress invariants (σ_{I} vs. σ_{II}, in kN m^{-1}, left column), normal stresses and scaled strain rate invariants (σ_{I} vs. $(1-d)^3 \dot{\epsilon}_{II}$, right column) in heavily damaged (d > 0.9) grid cells, at t = 57 min (during the fracture development, top row), t = 60 min (a few minutes after the fracture, middle row), and t = 90 min ($\sim$ 30 min after the fracture, bottom row). Color indicates the local damage. The strain rates are normalised to account for the non-linear dependency of the viscosity η on the damage parameter. The gradual alignment of the points in the σ_{I} vs. $(1-d)^3 \dot{\epsilon}_{II}$ diagram indicate the development of a linear-viscous stress-strain relationship over time.”

L276: A reference to the contrasting results is needed.

>> We add the reference to Ringeisen et al. (2019) for the VP model and to Bardet (1991), Balendran and Nemat-Nasser (1993), for granular materials.

L291: A reference for what is typical for granular material is needed (a textbook will suffice).

>> We added areference to the Bolton et al. (1986), describing the sawtooth model of granular dilatancy.

L316: This entire paragraph is a bit up-side-down to me. You start by saying the MEB is not good enough, for various reasons (begging the question of why you use it in the first place, actually) - and then you say how your new addition will not save it. A more natural way to write this is to first say that although the decohesive stress tensor can do some things it cannot fix everything, including etc.

>> We do not state that the MEB is not good enough. We mention the differences in behaviour with respect to the more commonly used VP models and discuss these differences in terms of potential limitations that should be taken into account in future model developments. We do believe that the use of several different models raises questions that would not be raised with the use of a single model, even if that model is better. Our community has suffered from a monopoly in approach with the standard VP model, until only very recently when new approaches were developed. This is made clear in the introduction of the revised manuscript.

We also believe that this discussion is made clearer in the revised manuscript by specifying in the abstract, at L84-90 and L180-L188 that we developed the generalized damage parameterization

in part to investigate the influence of the return algorithm on the simulated fractures.

L329: This paragraph is off topic, discussing experiments not introduced before and not relevant to the introduction of the decohesive stress tensor. Please remove.

>> We argue that this paragraph serves to put our results in context with other MEB model studies, which use different material parameters. In the revised manuscript, we widen the discussion to integrate the effect of grid resolution, sample aspect ratio, advection and heterogeneity, and clarify the context of this discussion.

L353: Now I'm confused, did you want to solve the ridging problem by introducing the decohesive stress? Again, a more natural way to present your results would be to first state what works and then what remains.

>> We now specify that the generalized damage parameterization modification is used to tackle issues that we raised on the damage parameterization in a previous paper (Plante et al. 2020) but also to investigate the influence of the return algorithm on the simulated fractures. The dominance of the post-fracture deformations in the MEB rheology is an important finding in our experiments, which contrasts with the behaviour in the VP and EVP rheologies. This is clarified in the conclusion at L443-449, but also in the abstract, at L84-L90 and at L180-L188 in the revised manuscript.

References:

Amitrano, D. and Helmstetter, A.: Brittle creep, damage and time to failure in rocks, Journal of Geophysical Research : Solid Earth, 111, B11 201, https://doi.org/10.1029/2005JB004252, 2006.

Balendran, B. and Nemat-Nasser, S.: Double sliding model for cyclic deformation of granular materials, including dilatancy effects, J. Mech. Phys. Solids, 41, 1993.

Bardet, J.: Orientation of shear bands in frictional soils, Journal of Engineering Mechanics - ASCE, 117, 1466–1484, https://doi.org/10.1061/(ASCE)0733-9399(1991)117:7(1466), 1991.

Bolton, M. D.: The strength and dilatancy of sands, Geotechnique, 36, 65–78, https://doi.org/10.1680/geot.1986.36.1.65, https://doi.org/10.1680/geot.1986.36.1.65, 1986.

Carrier, A., Got, J.-L., Peltier, A., Ferrazzini, V., Staudacher, T., Kowalski, P., and Boissier, P.: A damage model for volcanic edifices: Implications for edifice strength, magma pressure, and eruptive processes, Journal of Geophysical Research: Solid Earth, 120, 567–583, https://doi.org/10.1002/2014JB011485, 2015.

Dansereau, V., Weiss, J., Saramito, P., and Lattes, P.: A Maxwell elasto-brittle rheology for sea ice modelling, The Cryosphere, 10, 1339–1359, https://doi.org/10.5194/tc-10-1339-2016, 2016.

Dansereau, V.,Weiss, J., Saramito, P., Lattes, P., and Coche, E.: Ice bridges and ridges in the Maxwell-EB sea ice rheology, The Cryosphere, 11, 2033–2058, 2017.

Dansereau, V., V. D_emery, E. Berthier, J. Weiss, and L. Ponson.: Collective Damage Growth Controls Fault Orientation in Quasibrittle Compressive Failure, Phys. Rev. Lett., 122, 085,501, doi:10.1103/PhysRevLett.122.085501, 2019.

Duran, J., *Sands, Powders, and Grains: An Introduction to the Physics of Granular Materials* (translated by A. Reisinger). November 1999, Springer-Verlag New York, Inc., New York.

Leppäranta M.,: *The drift of sea ice*, Springer-Verlag Berlin Heidelberg, doi:10.1007/b138386, 2011.

Main, I. G.: A damage mechanics model for power-law creep and earthquake aftershock and foreshock sequences, Geophysical Journal International, 142, 151–161, https://doi.org/10.1046/j.1365-246x.2000.00136.x, 2000.

Plante, M., Tremblay, B., Losch, M., and Lemieux, J.-F.: Landfast sea ice material properties derived from ice bridge simulations using the Maxwell elasto-brittle rheology, The Cryosphere, 14, 2137–2157, https://doi.org/10.5194/tc-14-2137-2020, https://tc.copernicus.org/articles/14/2137/2020/, 2020.

Rampal, P., Bouillon, S., Ólason, E., and Morlighem, M.: neXtSIM: a new Lagrangian sea ice model, The Cryosphere, 10, 1055–1073, https://doi.org/10.5194/tc-10-1055-2016, 2016.

Rampal, P., Dansereau, V., Olason, E., Bouillon, S., Williams, T., Korosov, A., and Samaké, A.: On the multi-fractal scaling properties of sea ice deformation, The Cryosphere, 13, 2457–2474, https://doi.org/10.5194/tc-13-2457-2019, 2019.

Ringeisen, D., Losch, M., Tremblay, L. B., and Hutter, N.: Simulating intersection angles between conjugate faults in sea ice with different viscous–plastic rheologies, The Cryosphere, 13, 1167–1186, https://doi.org/10.5194/, 2019.

Ringeisen, D., Tremblay, 490 L. B., and Losch, M.: Non-normal flow rules affect fracture angles in sea ice viscous-plastic rheologies, The Cryosphere Discussions, 2020, 1–24, https://doi.org/10.5194/tc-2020-153, https://tc.copernicus.org/preprints/tc-2020-153/, 2020.

Weiss J. Drift, Deformation and Fracture of Sea Ice: A Perspective Across Scales. Netherlands: Springer, Dordrecht; 2013, p. 83. https://doi.org/10.1007/978-94-007-6202-2.

Weiss, J., Schulson, E. M., and Stern, H. L.: Sea ice rheology from in-situ, satellite and laboratory observations : Fracture and friction, Earth and Planetary Science Letters, 255, 1–8, https://doi.org/10.1016/j.epsl.2006.11.033, 2007.

Answers to tc-2020-354 RC4

May 6h, 2021

Note:

- The referee comments are shown in black,
- The authors answers are shown in blue,
- *Quoted texts from the revised manuscript are shown in italic and in dark blue.*
- Amendments made to the responses in the open discussion are shown in green

Please consider this an amendment to my review, RC3.

I now realise that the paper is fundamentally flawed and should be rejected/withdrawn.

The authors propose that super-critical stress be relaxed onto the failure envelope via a path different from the shortest distance to the origin in (σ_I, σ_{II}) space - as per figure 1. In order to do so they propose calculating the damage factor Ψ via equation (17) or (25, which has a typo). This, however, will not have the desired effect, because Ψ scales *d*, which then scales *all* the components of σ *equally*. Please consider equations (12), (8), (9), and (5) to see how changing *d* affects σ.

In other words, as long as *d* is a scalar, and not a tensor, then any form of Ψ will reduce the stress towards the origin - Ψ only determines how fast this happens.

For a more concrete example consider the stress change σ' -> σ_c in figure 1a. In order to change the stress in this manner, we need to reduce the shear stress but *increase* (in absolute value) the normal stress. This cannot be done by increasing *d*.

A generalised stress correction scheme, therefore, requires *d* to be a tensor, so that different components of the stress can change differently. This is not done here, and the scheme proposed simply does not do what the authors claim it does. Instead of taking a different path to the failure envelope, the proposed scheme takes the same path as the standard scheme but increases the damage too little for the stress to cease being super-critical. The proposed scheme is thus not usable and a paper discussing it is not warranted.

>> It is correct that the damage factor Psi is a scalar, but the reviewer missed the fact that we use a decohesive stress tensor to bring the stress back onto the yield curve, and which depends on the correction path angle (see Eqs 18-20, discussion on L150-161, Fig 1, and derivation below). This is emphasized in the revised manuscript at L204-207.

Therefore, the corrected normal stress invariant reads:

$\sigma_{Ic} = \Psi\sigma'_I + \sigma_{ID}$,

rather then $\sigma_{Ic} = \Psi\sigma'_I$, which was the reviewer's concern.

The components of the decohesive stress tensor are then retrieved using the yield criterion, such that:

$$\frac{c - \sigma_{IIc}}{\mu} = \Psi\sigma'_I + \sigma_{ID}$$

$$\sigma_{ID} = \frac{c - \sigma_{IIc}}{\mu} - \Psi\sigma'_I$$

Using the relation $\sigma_{IIc} = \Psi\sigma'_{II}$, we get Eq. 19 (where there was a typo):

$$\sigma_{ID} = \frac{c - \Psi(\sigma'_{II} + \mu\sigma'_I)}{\mu}$$

In which Ψ depends on the correction path angle. We can provide a more complete derivation in this thread if desired.

A generalized stress correction scheme for the MEB rheology: impact on the fracture angles and deformations

Mathieu Plante[1] and L. Bruno Tremblay[1]

[1]Department of Atmospheric and Oceanic Sciences, McGill University, Montréal, Québec, Canada

Correspondence: Mathieu Plante (mathieu.plante@mail.mcgill.ca)

Abstract. ~~A generalized damage parameterization is developed for the~~

The Maxwell Elasto-Brittle (MEB) rheology ~~that reduces the growth of residual errors associated with the~~ uses a damage parameterization to represent the brittle fracture of sea ice without involving plastic laws to constrain the sea-ice deformations. The MEB damage parameterization is based on a correction of super-critical stresses ~~. In the generalized parameterization, a~~ that binds the simulated stress to the yield criterion but leads to a growth of errors in the stress field. A generalized damage parameterization is developed to reduce this error growth and to investigate the influence of the super-critical stress correction scheme on the simulated sea-ice fractures, deformations and orientation of Linear Kinematic Features (LKFs). A decohesive stress tensor is used to ~~bring~~ correct the super-critical stresses ~~back~~ towards different points on the yield curve~~based on any correction path~~. The sensitivity of the simulated ~~material behaviour to the magnitude of the~~ sea-ice fractures and deformations to the decohesive stress tensor is investigated in uniaxial compression ~~simulations~~experiments. Results show that ~~while~~ the decohesive stress tensor influences the ~~short-term fracture deformation and orientation,~~ growth of residual errors associated with the correction of super-critical stresses, the orientation of the lines of fracture and the short-term deformation associated with the damage, but does not influence the long-term post-fracture ~~behaviour remains unchanged. Divergence first occurs when~~ sea-ice deformations. We show that when ice fractures, divergence first occurs while the elastic response is dominant~~followed by~~ , and convergence develops post-fracture ~~shear and convergence~~ in the longer-term when the viscous response dominates – contrary to laboratory experiment of granular flow and satellite imagery in the Arctic. The post-fracture deformations are shown to be dissociated from the fracture process itself, an important difference with classical Viscous Plastic (VP) models in which large deformations are governed by associative plastic laws. Using the generalized damage parameterization together with a stress correction path normal to the yield curve ~~brings the simulated fracture angles~~ reduces the growth of errors sufficiently for the production of longer-term simulations, with the added benefit of bringing the simulated LKF intersection half-angles closer to observations (from $40-50°$ to $35-45°$, compared to ~~$20-30°$~~ $15-25°$ in observations)~~and reduces the growth of errors sufficiently for the production of longer-term simulations~~.

Copyright statement.

1 Introduction

Sea ice is a thin layer of solid material that insulates the polar oceans from the cold atmosphere. When sea ice fractures and a lead ~~(or Linear Kinematic Features, LKFs)~~ opens, large heat and moisture fluxes take place between the ocean and the atmosphere, significantly affecting the polar meteorology on short time-scales and the climate system on long time-scales (Maykut, 1982; Ledley, 1988; Lüpkes et al., 2008; Li et al., 2020). The refreezing of leads ~~significantly~~ contributes to the sea ice mass balance (Wilchinsky et al., 2015; Itkin et al., 2018)~~, and~~ ; the associated brine rejection drives the thermohaline ocean circulation in the Arctic and vertical eddies in the ocean mixed layer (Kozo, 1983; Matsumura and Hasumi, 2008). As such, the production of accurate seasonal-to-decadal projections using coupled models requires an accurate representation of ~~sea ice leads. Furthermore, the presence and deformations along LKFs can influence the pressure on ships and increase the risk of besetting (??).The increased navigation through the Arctic passages (?Aksenov et al., 2017) thus calls for the development of high-resolution sea ice forecast products that capture the finer-scale lead structures (Jung et al., 2016).~~ sea-ice deformations along Linear Kinematic Features (LKFs).

As ~~sea ice~~ sea-ice models are moving to higher spatial resolutions, they become increasingly capable of resolving LKFs ~~(Hutter et al., 2019; ?). The simulation of the ice fractures yet represents a challenge~~(Hutter et al., 2018, 2021). The representation of smaller-scale fracture physics on the other hand yet remains a challenge, as most sea-ice models are based on a continuum approach and rely on parameterizations to relate sea-ice deformations and unresolved fractures. To this day, ~~most sea ice models simulate the motion of sea ice~~ this is most commonly done using plastic rheologies or modifications thereof ~~(Hibler, 1979; Hunke, 2001) . While several improvements were made on the numerics and efficiency of the methods used~~ (Hibler, 1979; Hunke and Dukowicz, 1997) , which have benefited from improved numerical scheme and efficiency to solve the highly non-linear momentum equation ~~(Hunke, 2001; Lemieux et al., 2008, 2014; Kimmritz et al., 2016; Koldunov et al., 2019), the physics governing the ice fracture remains mostly the same~~(Lemieux et al., 2008, 2014; Kimmritz et al., 2016; Koldunov et al., 2019). These models use plastic flow rules to represent the rate-invariance of sea-ice deformations at large spatio-temporal scale, in which the sea-ice can be considered ductile, but neglect the influence of the smaller-scale physics associated with the brittle fractures. A number of ~~rheologies have however~~ other rheologies have been developed over the years ~~in an attempt to simulate the observed~~ to relate the sea-ice deformations ~~(Tremblay and Mysak, 1997; Wilchinsky and Feltham, 2004; Schreyer et al., 2006; Sulsky and Peterson, 2011; Ramp . Among these new approaches, a damage parameterization~~ to the smaller-scale fracture physics (Tremblay and Mysak, 1997; Wilchinsky a . This brings a diversity of sea-ice rheologies with different physical and numerical framework that influence the representation of sea-ice deformations at different scales.

The Sea Ice Rheology Experiment (SIREx, Bouchat et al., 2021; Hutter et al., 2021), a coordinated effort between several ice-ocean modeling groups, assessed the pan-Arctic sea-ice deformation statistics simulated by different sea-ice rheologies. SIREx included the classical viscous-plastic (Hibler, 1979) and elastic-viscous-plastic (Hunke and Dukowicz, 1997) sea ice rheologies as well as the elastic-anisotropic (Wilchinsky and Feltham, 2004) and Maxwell-Elasto-Brittle (MEB, Dansereau et al., 2016) rheologies that include parameterizations of unresolved small scale physics. All participating sea ice models produced sea-ice deformation characteristics that have previously been associated with brittle behaviour, such as the scaling and spatio-temporal

coupling of sea-ice deformations (Bouchat et al., 2021), when run at sufficiently high resolution. The extent at which the inclusion of smaller-scale fracture physics improves this brittle behaviour thus remains an open question. Additionally, all rheologies produces similar angles between conjugate pairs of LKFs, a measure usually intimately related to the fracture mechanics and shear strength of a material (Bardet, 1991; Wang, 2007), showing a peek probability at 90° while the observed angles are in the range of 30-50° (Hutter et al., 2021). This calls for the improvement of sea-ice rheological models, such as modifications of the mechanical strength parameters and yield curve (Bouchat and Tremblay, 2017; Ringeisen et al., 2019; Dansereau et al. , the use of non-associated flow rules (in the case of classical plastic models, Ringeisen et al., 2021), or modifications of fine-scale fracture parameters (in the case of the EAP and MEB rheologies).

In the Maxwell Elasto-Brittle (MEB) rheology (Dansereau et al., 2016), the smaller-scale fracture physics is represented by a damage parameterization that was derived for rock mechanics and ~~seismology models (Amitrano et al., 1999; Amitrano and Helmstetter, 20~~ ~~was~~ seismic models (Amitrano et al., 1999; Amitrano and Helmstetter, 2006) and adapted for the large scale modelling of sea ice ~~(Girard et al., 2011; Bouillon and Rampal, 2015)~~(Girard et al., 2011; Bouillon and Rampal, 2015; Rampal et al., 2016) . This parameterization ~~uses~~ aims at representing the brittle character of sea-ice by using a damage parameter to represent the changes in material properties associated with fractures. This differs from parameterizations used in viscous plastic models in that the large-scale sea-ice deformations are not governed by plastic or granular flow rules. Instead, the sea-ice deformations in the MEB model are preconditioned by the presence of damage and the development of LKFs is associated with the far-field stress concentration response to local damage, leading to the propagation of the damage (i.e. fractures) in space (Dansereau et al., 2019). While still based on the continuum assumption, it allows for ~~fractures to propagate on short time-scales in~~ brittle fractures to influence the sea-ice ~~cover~~dynamics over shorter time-scales. It is currently used in the ~~Elasto-Brittle (EB Bouillon and Rampal, 2015; Rampal et al., 2016) and Maxwell Elasto-Brittle (MEB Dansereau et al., 2016) rheologies, implemented in the large scale~~ large-scale sea-ice Finite Element model neXtSIM (Rampal et al., 2019) and ~~, recently , in the Finite Difference McGill sea ice model~~ a finite difference version was recently implemented in the McGill Sea Ice Model Version 5 (McGill SIM5) (Plante et al., 2020).

The ~~damage parameterization is~~ MEB rheology being relatively new, ~~and it remains unclear to what extent differences in material behaviour are associated with the damage or to other rheological parameters. One known difference is the fracture development associated with local damage, stress concentration and damage propagation, rather than prescribed by an associative normal flow rule as in the standard VP models. The fracture angle simulated by the MEB and standard VP models are nonetheless in the same range ($\theta = 35 - 55°$, Dansereau et al., 2019; Hutter and Losch, 2020), which is larger than those derived from high-resolution satellite observations ($\theta = 20 - 45°$ Hutter et al., 2019) and in-situ observations ($\theta = 20 - 30°$ Marko and Th . In the standard VP model, modifications of the mechanical strength parameters (compressive and shear) and the use of non-associated flow rules lead to smaller fracture angles that are more in line with observations (Ringeisen et al., 2019, 2021) . In the MEB rheology, the fracture angles can be reduced by increasing~~ the extent to which the sea-ice deformations are sensitive to the numerical and material strength parameters have not been thoroughly tested yet. Nonetheless, the orientation of the simulated faults in uniaxial compression experiments are known to be sensitive to the angle of internal friction ~~or~~ and to the Poisson ratio (Dansereau et al., 2019). ~~These sensitivities suggest that modifications to the damage parameterization~~

could be used to bring the simulated fracture angles closer to observationsThis sensitivity is attributed to the influence of these parameters on the far-field stress concentration response to local damage, which determines the direction of the damage propagation. This suggests that the simulated angle of fracture may be sensitive to the exact choice of damage parameterization, but has not yet been tested.

The MEB rheology also presents some numerical challenges associated with the Additionally, while the neXtSIM model performed well compared to other SIREx models, the Lagrangian numerical scheme could also be responsible for the different scaling and localisation statistics (Bouchat et al., 2021). The Finite Difference implementation of the MEB rheology in the McGill SIM5 model, on the other hand, shows fast growth of residual errors associated with the damage parameterization at the grid scale – in ideal experiments – that significantly affect the post-fracture sea-ice deformations (Plante et al., 2020). These errors can be attributed to result from the stress correction scheme , a numerical tool used used in the MEB rheology to define the growth of damage and to bring the super-critical stresses back to the yield curve. Other To our knowledge, defining the damage in terms of the super-critical stress correction is new and unique to the EB and MEB sea-ice rheologies. For instance, most progressive damage models instead represent the damage parameter as a discrete function of the number of failure cycles (Main, 2000; Amitrano and Helmstetter, 2006; Carrier et al., 2015). In continuum damage mechanics, a damage potential derived the damage parameter is derived instead from thermodynamic laws (Murakami, 2012) is used to simulate the to simulate material fatigue. In the Elastic-Decohesive (ED) rheology, material damage is not parameterized but a decohesive strain rate explicitly represents the material discontinuity associated with the ice fracture and reduces the material strength of sea-ice, based on the orientation of the failure surface (Schreyer et al., 2006; Sulsky and Peterson, 2011).

In this paper, we present a generalization of the damage parameterization that reduces the in which a decohesive stress tensor is introduced in the stress correction scheme such that the super-critical stresses can be brought back to the yield curve following different stress correction paths in the stress invariant space. The generalization is used to reduce the growth of the residual errors associated with the stress correction and brings the simulated fracture angle of sea ice in simple tested in uniaxial loading experiments closer to observations. Inspired by the work of Schreyer et al. (2006) and (Sulsky and Peterson, 2011), we introduce a decohesive stress associated with the fracture of sea ice and test its influence to examine the influence of the stress correction on the simulated sea-ice fracture and deformationsin uniaxial loading experiments.

The paper is . The sensitivity of the simulated fracture angles to the decohesive stress tensor is also investigated to find the stress correction paths that present the added benefit of bringing the simulated fracture angles closer to observations.

This manuscript is organised as follows. In section 2, we present the MEB rheology and governing equations. The generalized stress correction scheme is described in section 3. The uniaxial loading experimental experiment set-up is presented in section 4 along with the definition of diagnostics used to quantify the growth of damage and the growth of residual errors. Results are presented in section 5, with a focus on the material behaviour in uniaxial compression experiments and its response to the changes in the damage parameterization. In section 6, we discuss the influence of the stress correction and seeded heterogeneityprovide a discussion on the generalized damage parameterization performance and other model sensitivities. Conclusions are summarized in section 7.

2 Model

2.1 Momentum and continuity equations

The simulations are run using the MEB model implemented on a Eulerian, Finite Difference Arakawa C-grid in the McGill ~~Sea Ice Model Version 5 (McGill SIM5, Tremblay and Mysak, 1997; Lemieux et al., 2008; Plante et al., 2020)~~SIM5 (Tremblay and Mysak, 19
. The vertically integrated 2D momentum equation for sea ice ~~, forced with surface friction only (i.e.~~ can be written as (ignoring the sea surface tilt, the ~~coriolis~~ Coriolis and the ice grounding terms)~~, can be written as~~:

$$\rho_i h \frac{\partial \boldsymbol{u}}{\partial t} = \nabla \cdot \boldsymbol{\sigma} + \boldsymbol{\tau}, \tag{1}$$

where ρ_i is the ice density, h is the mean ice thickness, $\boldsymbol{u}$ $(= u\hat{\boldsymbol{i}} + v\hat{\boldsymbol{j}})$ is the ice velocity vector, $\boldsymbol{\sigma}$ is the vertically integrated internal stress tensor and $\boldsymbol{\tau}$ is the net external surface stress from winds and ocean currents. This simplified formulation is appropriate for short term uniaxial loading experiments but can result in small errors in ice velocity when using a realistic model domain and forcing (Turnbull et al., 2017). Following ~~(Plante et al., 2020)~~Plante et al. (2020), we define the uniaxial loading by a surface wind stress $\boldsymbol{\tau}_a$ and prescribe an ocean at rest below the ice:

$$\boldsymbol{\tau} \approx \boldsymbol{\tau}_a - \rho_w C_{dw} |\boldsymbol{u}| \boldsymbol{u}, \tag{2}$$

where ρ_w is the water density, C_{dw} is the water drag coefficient and $\boldsymbol{u}$ is the sea ice velocity (see values in Table 1).

The prognostic equations for the mean ice thickness h (volume per grid cell area) and concentration A are written as:

$$\frac{\partial h}{\partial t} + \nabla \cdot (h\boldsymbol{u}) = 0, \tag{3}$$

$$\frac{\partial A}{\partial t} + \nabla \cdot (A\boldsymbol{u}) = 0, \tag{4}$$

where the thermodynamic source an sink terms are ignored.

2.2 Maxwell Elasto Brittle Rheology

The MEB model differs from classical sea-ice models in that it represents the brittle character of sea ice using a damage parameter to represent the effect of local fracture on the large-scale sea-ice material properties. The sea-ice deformations in the MEB model thus occur post-fracture, rather than simultaneously as in most sea-ice model using granular or plastic flow laws, and the formation of LKFs follows from the propagation of damage in space over short time-scales during the fracture process.

In the MEB rheology, the ice behaves as a visco-elastic material with a fast elastic response ~~and a viscous response~~ to forcing and a slower viscous response that act over a longer-time scale. The governing equation for this visco-elastic material can be written as (Dansereau et al., 2016, 2017; Plante et al., 2020):

$$\frac{\partial \boldsymbol{\sigma}}{\partial t} + \frac{1}{\lambda}\boldsymbol{\sigma} = E\mathbf{C} : \dot{\boldsymbol{\epsilon}}, \tag{5}$$

where E is the elastic stiffness defined as the vertically integrated Young Modulus of sea ice, λ is the viscous relaxation time-scale, $\mathbf{C}$ is the ~~elastic tensor~~ (fourth order) elastic tensor, ":" denotes the inner double tensor product and $\dot{\epsilon}$ is the (second order) strain rate tensor. The ~~elastic tensor $\mathbf{C}$ and strain rate tensor $\dot{\epsilon}$~~ tensors C and $\dot{\epsilon}$ in the right hand side of Eq. 5 can be written ~~is matrix form~~ in matrix form by representing the 3 independent components of the stress and strain tensors in a vector (see Rice, 2010), and the 9 independent components of the elastic modulus tensor in a 3x3 matrix, as:

$$\mathbf{C} = \frac{1}{1-\nu^2}\begin{pmatrix} 1 & \nu & 0 \\ \nu & 1 & 0 \\ 0 & 0 & 1-\nu \end{pmatrix}, \tag{6}$$

$$\begin{pmatrix} \dot{\epsilon}_{xx} \\ \dot{\epsilon}_{yy} \\ \dot{\epsilon}_{xy} \end{pmatrix} = \begin{pmatrix} \frac{\partial u}{\partial x} \\ \frac{\partial v}{\partial y} \\ \frac{1}{2}\left(\frac{\partial u}{\partial y} + \frac{\partial v}{\partial x}\right) \end{pmatrix} \tag{7}$$

where ν ($= 0.33$) is the Poisson ratio, which defines the relative amount of deformation on the plane parallel to the loading.

The relative importance of the elastic and viscous components (first and second terms on the left hand side in Eq. 5) are determined by the magnitude of the elastic modulus E and viscous relaxation time-scale λ. E and λ are functions of the ice thickness, concentration and damage~~resulting in dominant elastic component for small deformations (undamaged ice) and dominant viscous component for large deformations (heavily fracturedice)~~, such that the elastic term dominates when the ice is undamaged while the viscous term dominates when the ice is heavily fractured. The elastic modulus E and viscous relaxation time-scale λ are written as:

$$E = Yhe^{-a(1-A)}(1-d), \tag{8}$$

$$\lambda = \lambda_0(1-d)^{\alpha-1}, \tag{9}$$

where Y (= 1 GPa) is the Young Modulus of undeformed sea ice, d is the damage parameter ($0 < d < 1$), a (= 20) is the standard ~~parameter ruling the dependency of the material strength properties on sea-ice concentration~~ ice concentration parameter (Hibler, 1979; Rampal et al., 2016), λ_0 ($= 10^5$s, $\approx$1 day) is the viscous relaxation time scale for undamaged sea ice and α is a parameter ~~ruling~~ defining the post-fracture transition to the viscous regime. This damage-based transition to post-fracture viscosity represents a simplification of the observed plasticity (rate-independence) of sea-ice deformations (Coon et al., 1974; Tuhkuri and Lensu, 2002).

2.3 Yield criterion

Damage (or fracture) occurs when the internal stress state exceeds the Mohr-Coulomb failure criterion,

$$F(\sigma) = \sigma_{II} + \mu\sigma_I - c < 0, \tag{10}$$

where,

$$\sigma_I = \frac{\sigma_{xx} + \sigma_{yy}}{2}, \tag{11}$$

$$\sigma_{II} = \sqrt{\left(\frac{\sigma_{xx} + \sigma_{yy}}{2}\right)^2 + \sigma_{xy}^2}, \tag{12}$$

where σ_I is the isotropic normal stress invariant (compression defined as negative), σ_{II} is the maximum shear stress invariant, (σ_{xx},σ_{yy},σ_{xy}) are the components of the stress tensor, μ ($= \sin\phi$) is the coefficient of internal friction of ~~ice~~sea-ice, ϕ (= 45°) is the angle of internal friction, and c is the vertically integrated cohesion, defined as~~:~~,

$$c = c_0 h e^{-a(1-A)}, \tag{13}$$

where c_0 (= 10 kN m^{-2}) is the cohesion of sea ice derived from observations (Sodhi, 1997; Tremblay and Hakakian, 2006; Plante et al., 2020) or laboratory experiments (Timco and Weeks, 2010). No compressive or tensile strength cut-off are used in this analysis. The reader is referred to Table 1 for a list of default model parameters.

2.4 Damage parameterization

The prognostic equation for the damage parameter d in the standard MEB rheology is parameterized using a relaxation term with time scale T_d ($= 1$ s) as:

$$\frac{\partial d}{\partial t} = \frac{(1-\Psi)(1-d)}{T_d}, \tag{14}$$

where

$$\Psi = \frac{\boldsymbol{\sigma}_c}{\boldsymbol{\sigma}'} = \min\left(1, \frac{c}{\sigma'_{II} + \mu\sigma'_I}\right), \tag{15}$$

is a damage factor ($0 < \Psi < 1$), $\boldsymbol{\sigma}_c$ is the critical stress lying on the yield curve and $\boldsymbol{\sigma}'$ is the uncorrected stress state lying outside of the yield curve. Thermodynamic healing and ~~advection~~ the advection of damage are neglected as we are focusing on the ice fracture~~.~~, which occurs at a timescale (seconds) much shorter than the healing and advection timescales (hours). Adding these terms does not change the results and conclusions presented in this paper but increases the localisation of the ice fractures with higher damage values that in turn increases ridging. These terms should be included in longer-term integration of the MEB model.

When the ice fractures, the damage factor Ψ is used to scale the super-critical stresses back towards the yield curve. The prognostic equation for the temporal evolution of the super-critical stress tensor $\boldsymbol{\sigma}'$ is written as a relaxation equation of the same form as in Eq. 14:

$$\frac{\partial \boldsymbol{\sigma}'}{\partial t} = -\frac{(1-\Psi)\boldsymbol{\sigma}'}{T_d}. \tag{16}$$

This stress correction scheme corresponds to scaling all the individual stress components by the factor Ψ, such that the stress state is corrected back onto the yield curve in the stress invariant space by following a line passing through the origin. This results in a dependency of the stress correction magnitude and of the damage on the super-critical stress state: i.e., the stress correction path becomes increasingly parallel to the yield curve for increasing compressive super-critical stresses, which also increases the numerical errors (Plante et al., 2020). We hereafter refer to this scheme as the "standard stress correction".

3 Generalized stress correction

We propose a generalized damage parameterization where the super-critical stresses are corrected back to the yield curve along a line oriented at any angle γ from the y-axis in the stress invariant space (see Fig. 1). ~~To this end, we chose to~~ This generalization is developed with the goal of reducing the growth rate of the numerical errors in the MEB model by removing the dependency of the stress correction path on the super-critical stress state, while keeping the changes in the damage parameterization to a minimum so that it can be easily added to other MEB model implementations (and other damage-based models). In the MEB model, the exact path along which the super-critical stresses is returned to the yield curve is not known a priori, as the stress state never exceeds the yield criterion in reality. The proposed generalization allows to investigate the influence of the super-critical stress correction path angle on the simulated fractures and deformations. Other physically meaningful modifications of the stress correction that are based on thermodynamics principles are left for future work (see for instance Murakami, 2012) .

We define the damage factor in the generalized damage parameterization in terms of the shear stress invariant only, as:

$$\Psi = \frac{\sigma_{IIc}}{\sigma'_{II}}, \tag{17}$$

where σ_{IIc} is the critical shear stress invariant. The equation defining the stress correction path with angle γ (see Fig 1) can be written as:

$$\sigma_{II} = (1/\tan(\gamma))\sigma_I + B, \tag{18}$$

where B $(= \sigma'_{II} - 1/\tan(\gamma)\sigma'_I)$ is defined from the super-critical stress state (σ'). The critical shear stress invariant (σ_{IIc} ~~is defined by~~) is then defined as the intersection point between the ~~correction path and the~~ yield curve (~~see Fig 1). After some algebra, we obtain:~~ Eq. 10) and the stress correction path (18),

$$\sigma_{IIc} = \frac{c + \mu\tan(\gamma)\sigma'_{II} - \mu\sigma'_I}{1 + \mu\tan(\gamma)}. \tag{19}$$

The damage factor can then be written in terms of the super-critical stress state invariants (σ'_I,σ'_{II}), the correction path angle γ and the coefficient of internal friction μ, as:

$$\Psi = \frac{c + \mu\tan(\gamma)\sigma'_{II} - \mu\sigma'_I}{(1 + \mu\tan(\gamma))\sigma'_{II}}. \tag{20}$$

In this manner, the correction of super-critical stresses can follow any ~~line~~ path in the stress invariant space provided that the damage increases when ice fractures ($\Psi < 1$, or $\gamma < 90°$). ~~The generalized formulation now allows for the use of~~ This

formulation can also be used with a yield curve ~~without cohesion (~~with zero isotropic tensile strength (i.e. $c = 0$ kN m^{-1}),
~~something that is not possible in~~ as opposed to the standard parameterization ~~otherwise Ψ is identically equal to 0~~ in which case any super-critical stress state is returned to the origin (see Eq. 15 when $c = 0$ N m^{-}1).

Note that using a stress correction path other than the standard path to the origin means that the corrected normal stress differs from the scaled super-critical stress $\Psi\sigma'_I$. We define this difference as the decohesive stress tensor ~~needed to for the corrected stress to follow the stress correction path γ (see Fig. 1)~~(see Fig. 1), which is added to the damage parameterization to keep the corrected stress state on a given stress correction path. This effectively changes the stress correction while keeping the scalar definition of the damage parameter. The stress correction equation (Eq. 16) ~~then becomes:~~ in the generalized damage parameterization then becomes,

$$\frac{\partial \boldsymbol{\sigma}'}{\partial t} = -\frac{(1-\Psi)\boldsymbol{\sigma}' + \boldsymbol{\sigma}_D}{T_d}., \tag{21}$$

~~The~~ and the invariants of the decohesive stress tensor (σ_{ID},σ_{IID}) are ~~therefore written~~ now defined as:

$$\sigma_{ID} = \sigma_{Ic} - \Psi\sigma'_I = \frac{c - \Psi(\sigma'_{II} - \mu\sigma'_I)}{\mu}, \tag{22}$$

$$\sigma_{IID} = 0, \text{ (by definition).} \tag{23}$$

When $\tan\gamma = \sigma'_I/\sigma'_{II}$ and $\sigma_{ID} = \sigma_{IID} = 0$, we obtain the standard damage parameterization of Dansereau et al. (2016)~~as a special case where the stress correction path depends on the super-critical stress state.~~ .

Note that the decohesive stress tensor used in this parameterization has a similar role as the decohesive strain rates used in the Elastic-Decohesive model ~~Schreyer et al. (2006), in that they both determine the change in stress state associated with the development of a fracture . In the present scheme, $\boldsymbol{\sigma}_D$~~ (Schreyer et al., 2006). In Schreyer et al. (2006), the decohesive strain represents the discontinuity in sea-ice displacement associated with a fracture and relaxes the effective stress rates. It is derived from ~~the stress correction path, while the decohesive strain rate in Schreyer et al. (2006) is derived from the opening of a lead based on granular theory~~a decohesion function that depends on the mode of failure. Here, we do not define the strain discontinuity associated with the fractures, but use the decohesive stress tensor $\boldsymbol{\sigma}_D$ to prescribe the orientation at which the stress state is relaxed back onto the yield curve. This only indirectly influences the local strain rate via the constitutive equation.

3.1 Projected error

The error $\delta\Psi$ on the damage factor $\Psi(\sigma'_I, \sigma'_{II})$ can be written as (Plante et al., 2020):

$$\delta\Psi = \sqrt{\left(\frac{\partial\Psi}{\partial\sigma'_I}\right)^2 \delta\sigma'^2_I + \left(\frac{\partial\Psi}{\partial\sigma'_{II}}\right)^2 \delta\sigma'^2_{II}}, \tag{24}$$

where ($\delta\sigma'_I$,$\delta\sigma'_{II}$) are the errors ~~on~~ of the calculated stress invariants. ~~Expanding the derivative terms (using~~ Using Eq. 21 ~~)~~ and re-writing $\delta\sigma'_I$ and $\delta\sigma'_{II}$ in terms of the relative error ϵ (i.e., $\delta\sigma'_I = \epsilon\sigma'_I$, $\delta\sigma'_{II} = \epsilon\sigma'_{II}$), we obtain:

$$\delta\Psi = \sqrt{\frac{\mu^2}{(1+\mu\tan(\gamma))^2\sigma'^2_{II}}\epsilon^2\sigma'^2_I + \frac{(c-\mu\sigma'_I)^2}{(1+\mu\tan(\gamma))^2\sigma'^4_{II}}\epsilon^2\sigma'^2_{II}}, \tag{25}$$

$$= \Psi\epsilon\sqrt{\frac{\mu^2\sigma'^2_I + (c-\mu\sigma'_I)^2}{(c+\mu\tan(\gamma)\sigma'_{II}-\mu\sigma'_I)^2}}, \tag{26}$$

$$= \Psi\epsilon R \tag{27}$$

where R is the error amplification ratio.

~~Assuming~~ Given that the uncorrected stress is close to the yield criterion (i.e. $\sigma'_{II} + \mu\sigma'_I - c \sim 0$), ~~this relation indicates that~~ the error amplification ratio R ~~goes to infinity if:~~ tends to infinity for,

$$\tan(\gamma) = -1/\mu, \tag{28}$$

which corresponds to a path that runs parallel to the yield curve. This result is consistent with the instabilities in the standard stress correction scheme during ridging reported in Plante et al. (2020), given that a line passing through the origin is nearly parallel to the ~~Mohr-Coulomb~~ Mohr-Coulomb yield curve for large compressive stresses. In contrast, the path that maximizes the denominator (smallest error growth) has $\gamma = 90°$. This path, however, ~~correspond~~ corresponds to $\Psi = 1$ and does not create damage. The possible stress correction path angles γ thus lie in the range $\arctan(-1/\mu) < \theta < 90°$.

Note that the error amplification ratio R is small for $\sigma_I < 0$, but becomes infinitely large at the yield curve tip when σ'_{II} approaches 0 (see Eq. 25). This behaviour is opposite to that of the standard stress correction scheme, which has small R values in tension and large values in compression (Plante et al., 2020). ~~To minimize the errors for all stress states, we blend the two~~ For this reason, we use both schemes (i.e. Eq. 20 in compression and Eq. 15 in tension, see Fig. 1b) ~~. We~~ and set the transition between the two schemes at the points where ~~they are both equal~~ their paths are the same (i.e., at $\sigma'_I/\sigma'_{II} = \tan\gamma$, ~~see~~ green line in Fig 1b). The damage factor is then defined as:

$$\Psi = \begin{cases} \frac{c+\mu\gamma\sigma'_{II}-\mu\sigma'_I}{(1+\mu\gamma)\sigma'_{II}}, & \text{if } \sigma'_I < \sigma'_{II}\tan\gamma, \\ \frac{c}{\sigma'_{II}+\mu\sigma'_I}, & \text{otherwise.} \end{cases} \tag{29}$$

4 Methods

4.1 ~~Numerical approaches~~Experiment setup

~~The MEB model is implemented in the McGill Sea Ice Model Version 5 (McGill SIM5) using an Eulerian, 2nd order finite difference numerical scheme (Tremblay and Mysak, 1997; Lemieux et al., 2014; Plante et al., 2020). The equations are discretized in space using an Arakawa C-grid and in time using a semi-implicit backward Euler scheme (Plante et al., 2020) . A solution to the non-linear momentum and constitutive equations (Eqs. 1 and 5) is found using a Picard solver. The Picard~~

~~solver uses an outer loop in which the equations are linearized and solved at each iteration using a preconditioned Flexible General Minimum RESidual method (FGMRES, Lemieux et al., 2008). The non-linear terms are then updated and the linear problem solved again until the residual error ϵ_{res}, defined as the L2-norm of the solution vector, is lower than 10^{-8} N/m^2. The prognostic equations for the tracers (Eq. 3, 4 and 14) are updated within the outer loop iteration using an IMplicit-EXplicit (IMEX) approach (Lemieux et al., 2014). The reader is referred to Plante et al. (2020) for more details.~~

4.2 ~~Experiment setup~~

~~Following Ringeisen et al. (2019); Dansereau et al. (2019); Herman (2016), we present results from idealized uniaxial loading experiments and~~ We test the numerical and material behaviour of the MEB model and the generalized damage parameterization in uniaxial compression experiments. Uniaxial experiments are designed to present conditions similar to those in laboratory experiments and have been used with MEB (Dansereau et al., 2016), VP (Ringeisen et al., 2019) and Discrete Element (Herman, 2016) models to assess ice fracture characteristics, LKF angles and intermittency. In this analysis, we use the experiment designed by (Ringeisen et al., 2019) to test the sensitivity of the residual error growth, sea-ice deformation and LKF orientation on the correction path angle γ in the generalized stress correction scheme. The model domain is 250 x 100 km ~~(~~with 1km ~~resolution), with sea ice of~~ spatial resolution. The initial conditions are 1m ice thickness and 100% concentration in the middle 60 km of the domain ~~and~~ with two narrow bands of open water (20 km width) on each sides (Fig. 2). A ~~solid~~ solid-wall, Dirichlet boundary condition ($u = v = 0$) is used at the bottom, and ~~open~~ open-water, Neumann boundary conditions ($\partial u/\partial n = 0$) are used on the top and sides. In all experiments, the forcing is specified by a ~~surface stress τ_a~~ downward surface stress $\boldsymbol{\tau_a}$ (see Eq. 2) over the entire domain. This differs from Ringeisen et al. (2019) and Dansereau et al. (2016) where the upper boundary is represented by a moving wall acting as external forcing. The ~~forcing~~ magnitude of τ_a is ramped up from 0 to 0.60 N/m^2 (corresponding to $\sim$20 m/s winds or $\sim$0.33 m/s surface currents) in a 2h period, and then remains constant.

4.2 ~~Diagnostics definitions~~

Note that all simulations are performed without including heterogeneity in order to clearly identify the model performance (both numerics and physics), unless specified otherwise. This allows to quantify the growth of residual numerical errors in a problem with full symmetry and their impact on the simulated LKF orientation and post-fracture sea-ice deformations.

4.2 Numerical approaches

The MEB model is implemented in the McGill Sea Ice Model Version 5 (McGill SIM5) using a Eulerian, 2nd order finite difference numerical scheme (Tremblay and Mysak, 1997; Lemieux et al., 2014; Plante et al., 2020). The equations are discretized in space using an Arakawa C-grid and in time using a semi-implicit backward Euler scheme (Plante et al., 2020). A solution to the non-linear momentum and constitutive equations (Eqs. 1 and 5) is found using a Picard solver. The Picard solver uses an outer loop in which the equations are linearized and solved at each iteration using a preconditioned Flexible General Minimum RESidual method (FGMRES, Lemieux et al., 2008). The non-linear terms are then updated and the linear problem solved

again until the residual error ϵ_{res}, defined as the L2-norm of the solution vector, is lower than 10^{-8} N/m^2 (Lemieux et al., 2014, for details). The prognostic equations for the tracers (Eq. 3, 4 and 14) are updated within the outer loop iteration using an IMplicit-EXplicit (IMEX) approach (Lemieux et al., 2014). The reader is referred to Plante et al. (2020) for more details.

4.3 Diagnostics

4.3.1 Field asymmetry

We monitor the ~~growth~~ influence of the residual ~~error~~ errors on the model solution in the simulations using a normalised domain-integrated asymmetry factor (ϵ_{asym}) in the maximum shear stress invariant field (σ_{II})~~,~~. This diagnostic measures the asymmetry in the model solution about the y-axis (the vertical center line) and represents a measure of the numerical accuracy given that the model equations, initial conditions and boundary conditions are all fully symmetric. The asymmetry factor is defined as:

$$\epsilon_{asym} = \frac{\sum_{i=a}^{b}\sum_{j=1}^{ny}|\sigma_{II}(i,j)-\sigma_{II}(nx-i,j)|}{\sum_{i=a}^{b}\sum_{j=1}^{ny}|\sigma_{II}(i,j)|}\frac{\sum_{i=a}^{b}\sum_{j=1}^{ny}|(\sigma_{II})_{i,j}-(\sigma_{II})_{nx-i,j}|}{\sum_{i=a}^{b}\sum_{j=1}^{ny}|(\sigma_{II})_{i,j}}, \tag{30}$$

where (i,j) are the x-y grid indices respectively, (nx,ny) are the number of grid cells in the x and y-directions and (a,b) are the indices of the first and last ice-covered grid cells on the x-axis.

Note that the field asymmetry measures the degradation of the originally fully symmetric problem as numerical errors are integrated, and includes the physical response to the integrated errors. This is in contrast with the residual error amplification ratio R, which is a measure of the local amplification of the residual error by the damage parameterization at a given time-step. The maximum R values in the domain at each time-step (R_{max}) is also shown below to visualise the contribution of the damage parameterization to the growth of the residual errors.

4.3.2 Damage activity

We ~~define the~~ quantify the development of fractures in the experiments using the damage activity D, defined as the total damage integrated over the original ice domain in a ~~1 minute interval~~ given time interval Δ (= 60 s):

$$D = \sum_{i=a}^{b}\sum_{j=1}^{ny}\frac{d(i,j)^{t+30s}-d(i,j)^{t-30s}}{60s}\frac{d_{i,j}^{t+\Delta/2}-d_{i,j}^{t-\Delta/2}}{\Delta}. \tag{31}$$

This parameter is analog to the damage rate in ~~(Dansereau et al., 2016, 2017)~~Dansereau et al. (2016, 2017) and is used to identify the time at which the ice fractures. Note that this definition of damage activity (or damage rate) emphasizes activity in undamaged ice (i.e. new fractures) and is not sensitive to activity in already heavily damaged ice.

4.3.3 Fracture angle

~~When loaded in uniaxial compression, a granular material fails in diamond-shaped shear fractures (e.g. see Marko and Thomson, 1977; Rin~~

~~. We~~ The angles between conjugate LKFs in the Arctic are often discussed in relation with the orientation of the smaller-scale

brittle fractures observed in laboratory under uniaxial compression loads (i.e., Marko and Thomson, 1977; Schulson, 2004). The orientation of such compressive-shear fractures is often related to brittle fracture theories (e.g. to the development of wing cracks, Schu and in terms of granular properties such as Coulombic friction or dilatancy (Erlingsson, 1988; Tremblay and Mysak, 1997; Overland et al., .

Here, we define the fracture angle θ as the angle between the y-axis and the fracture lines (see Fig. 2). ~~The orientation of these fracture lines have been measured in laboratory using in uniaxial loading experiments . Several theories were developed to relate the fracture angle in terms of material parameters. The most common is~~ , and compare the simulated fracture angles in our experiments to two theories that are often used to describe the orientation of fractures: the Mohr-Coulomb fracture theory and the Roscoe theory of dilatancy. Widely used in geoscience and engineering, the Mohr-Coulomb theory (Coulomb, 1773; Mohr, 1900) ~~, where the fracture angle is related~~ relates the orientation of fractures to the angle of internal friction, as:

$$\theta = \frac{\pi}{4} - \frac{\phi}{2}. \tag{32}$$

~~This theory tends to underestimate the fracture angle of granular materials in laboratory experiments (Bardet, 1991). In the Roscoe (1970)~~ In the Roscoe (Roscoe, 1970) theory, the fracture angle is defined instead in terms of the angle of dilatancy (δ) of the granular material:

$$\theta = \frac{\pi}{4} - \frac{\delta}{2}. \tag{33}$$

If $\delta = \phi$, the two theories give the same fracture angle θ. In general, the fracture angle in geomaterial and soils falls between values predicted by the Mohr-Coulomb and Roscoe theories with zero dilatancy ($\delta = 0$) (Arthur et al., 1977; Bardet, 1991).

In our experiment, the fracture angle is calculated graphically for each individual simulation. We define the uncertainty as $\pm\tan(W/L) \sim \pm 2°$, where W is the fracture width (typically a few grid cells wide~~in our results~~, or $\sim$ 2-5 km) and L is the fracture length ($\sim$ 45 km). This error increases to $\pm 6°$ for the few cases where the fracture is not ~~well defined~~as localized.

5 Results

5.1 Control simulation: standard damage parameterization

In the control simulation, a pair of conjugate ~~fracture lines~~ LKFs first appear when the surface forcing $\tau_a = 0.29$ N ~~/m~~m^{-2}, along with secondary ~~fracture~~ lines that are the results of interactions between the ice floe and the solid boundary that extends across the full width of the domain at the base (Fig. 3). All ~~fracture lines~~ LKFs are oriented at 39° from the y-axis, smaller than reported by Dansereau et al. (2019) using a Finite Element implementation of the same model ($\theta = \sim 43°$) and ~~in the high range~~ higher than seen in observations ~~(θ = ~20-40° Marko and Thomson, 1977; Hibler III and Schulson, 2000; Schulson, 2004; Hutter and Los~~ (θ = ~15-25° Marko and Thomson, 1977; Hibler III and Schulson, 2000; Schulson, 2004; Hutter et al., 2021). This orientation also falls in between that predicted by the Mohr-Coulomb ($\theta = 22.5°$) and Roscoe theories ($\theta = 45°$ when $\delta = 0$), in accord with the common observation that both the angle of internal friction and the dilatancy (δ) are important in defining the ~~fracture~~ fault orientation (Arthur et al., 1977; Vardoulakis, 1980; Balendran and Nemat-Nasser, 1993).

~~When the ice fractures, the initial response is mostly elastic with divergence along the fracture line. The resulting stress concentration~~ The deformation along the fully developed LKFs in our experiment is mostly shear and convergence (i.e. ridging, Fig. 3c-d). This contrasts with the early stage of the LKF development during which the material response to the new damage is elastic and shows mostly divergent deformations (see the positive strain rates in Fig. 4b). This elastic response to damage influences the propagation of the ~~fracture in space over~~ fractures in space at short time-scales (seconds) governed by the elastic waves speed. The convergent deformations only develops over a longer time-scales as the sea-ice deformation continues ~~to occur~~ post-fracture in the damaged ice and ~~, over time, the response transitions from elastic to~~ the deformation transitions from the elastic- to that viscous-dominated ~~as the Maxwell viscosity dissipates the elastic stresses and creates permanent viscous deformations~~regime. This transition is clearly seen in the development of a linear dependence between stress and strain-rate invariants (scaled by $(1-d)^3$), where the slope corresponds to the viscosity (see ~~for instance 4 e,f, i~~the transition from 4 b,d, to f). The simulation reaches steady state with deformations that are fully viscous and localized in the heaviest damage areas (Fig. 4g-i). This causes a predominance of shear and convergence deformation along the ~~fracture line~~ LKFs throughout the simulation.

The asymmetries in the solution are very small at the beginning of the simulation (t ~~$\leq 57min$~~ $\leq$ 57 min), and do not grow until fractures occur (Fig. 5a-b). As the ~~fractures~~ LKFs develop, small errors grow rapidly with ~~ϵ_{asym}~~ ϵ_{asym} increasing in large steps crossing multiple orders of magnitude. Note that the model is always iterated to convergence with a strict residual error tolerance (~~$\epsilon_{res} = 10^{-6} Nm^{-2}$~~ $\epsilon_{res} = 10^{-8}$ N m^{-2}). The steep growth in ϵ_{asym} ~~are~~ is associated with large ~~values of damage~~ (> 1) values of the error amplification ratio R (~~reaching~~ see Eq. 27), and reach $\sim$20 ~~,~~ in the control simulation (Fig. 5b). Since ϵ_{asym} is a domain-integrated quantity, it increases in time following large local error growths R. This illustrates the long-range and long-term influence of residual errors, which act on the development of the future fractures. Note that ϵ_{asym} saturates when the σ_{II} field is no longer symmetric, and becomes insensitive to additional error growth. We assess the precision of the solution using the maximum error amplification ratio ~~R_{max}, which indicate~~ R_{max}, which indicates the level of amplification of residual errors in the simulations, at times by more than one order of magnitude locally (~~$R_{max} > 10$~~ $R_{max} > 10$).

5.2 Generalized stress correction

The generalized damage parameterization reduces the growth of residual errors, with decreasing asymmetry factor and error amplification ratio ~~R_{max}~~ R_{max} for increasing path angle γ (Fig. 6~~a). This~~). In particular, using $\gamma > 0°$ stabilises the damage parameterization and eliminate the large spikes in R_{max} seen in the control simulation or when using $\gamma < 0°$, where the residual error increases by up to two orders of magnitude locally. The increased stability results in an overall ~~reduction~~ smaller and smoother growth of the asymmetry factor ϵ_{asym} (Fig. 6~~b~~a), allowing for ~~the production of~~ longer-term symmetrical simulations that include post-fracture deformations. ~~This improvementis only significant when using $\gamma > 0$. For $\gamma < 0$, the maximum error amplification ratio R_{max} remains important with periods when the residual error increases by up to two orders of magnitude locally.~~ Note that despite this improvement, the asymmetry factor ϵ_{asym} still grows over time as the simulations remain sensitive to the residual errors in heavily damaged ice, due to the non-linear relationship between the sea ice deformation and the damage.

This effect is less important when using large correction path angles ($\gamma > 45°$) due to a slower LKF development, as discussed below.

Results show that the ~~fracture angle~~ LKF orientation is sensitive to the decohesive stress tensor, with decreasing ~~fracture~~ angle θ for increasing stress correction path angle γ (Fig. 7). This finding is in line with results from Dansereau et al. (2019), where the ~~fracture angle~~ orientation of faults was related to the far-field stress associated with the collective damage. In the MEB model, the far-field stresses directly ~~depends on~~ depend on the corrected stress state, ~~including~~ which includes $\boldsymbol{\sigma}_D$ in the generalized damage parameterization. Increasing the correction path angle γ reduces the ~~fracture angles~~LKF angles, in better agreement to observations.

~~Along the fracture lines, the~~ The correction path angle γ influences the time-integration required to reach the same damage and deformation rates (Fig. 8) ~~. This~~ along the LKFs. This is due to the fact that increasing the angle γ reduces the amount of damage for the same super-critical stress state because the stress correction path approaches the horizontal and Ψ is closer to 1. The simulated ice deformations are otherwise mostly insensitive to the correction path angle; i.e. all simulations have divergence during the initial elastic response when the ice fractures followed by a transition to viscous deformations where shear and convergence deformations are predominant (Fig. 8a). In contrast with ~~results from the VP model and from~~ plastic flow (Ringeisen et al., 2019, 2021) or typical granular material behaviour (Balendran and Nemat-Nasser, 1993; Tremblay and Mysak, 1997) , divergent post-fracture deformation is only present when tensile stresses develop, e.g. at the intersection between conjugate ~~lines of fracture~~LKFs. This behaviour stems from the use of post-fracture viscosity to represent the large-scale sea-ice deformations, and differs from classical VP model, which represent the observed plasticity of sea-ice deformations at the macro-scale (Coon et al., 1974; Tuhkuri and Lensu, 2002) but do not represent the brittle component of the fractures nor discontinuities in material properties.

5.3 Sensitivity to ϕ and ν

Repeating the experiment using different angles of internal friction (ϕ) shows that the ~~fracture angle decreases~~ LKF orientations decrease with increasing ϕ. The simulated ~~fracture angles~~ angles θ fall within the envelope from the Mohr-Coulomb and Roscoe theories, except for small angles of internal friction ($\phi < 20°$), a value that is rarely observed for granular materials (Fig. 9). Note that the sensitivity of the ~~fracture angle~~ LKF orientation to the coefficient of internal friction also disappears for small angles of internal friction ($\phi < 20°$) when using a large correction path angle ($\gamma = 60°$ in Fig. 7). When both the stress correction path and the yield criterion ~~approaches~~ approach the horizontal, fracture yields large stress corrections but small damage increases (i.e., $\Psi = 1$), such that the ~~angle of fracture is~~ LKF orientation is mostly governed by the stress correction and ~~is weakly sensitive~~ weakly sensitive to other model parameters. Based on these results, we suggest the use of a correction path that is normal to the yield criterion ($\gamma = \arctan\mu$, see black points in Fig. 9).

Decreasing the angle of internal friction reduces the shear strength of sea ice for a given normal stress, such that the fracture develops earlier in the simulation (i.e. under smaller surface forcing, Fig. 10). It also reduces the divergence associated with the elastic response when ice fractures and ~~increase~~ increases the convergence in the post-fracture viscous regime. This result

is typical for granular material, with smaller ~~fracture angles~~ fault orientations (larger angles of internal friction) associated with larger angles of dilatancy ~~and divergence during the fracture development~~Bolton (e.g. the sawtooth model, 1986)).

The ~~fracture angle~~ orientation of LKFs is not sensitive to the Poisson ratio when the generalized stress correction scheme is used with a fixed stress correction path angle γ (Fig 11). This is in contrast with simulations using the standard stress correction scheme, where the fracture angle decreases with increasing ν ~~(see blue points in Fig. 11, and also in Dansereau et al., 2019)~~ (see blue points in Fig. 11, and Dansereau et al., 2019). Note that the Poisson ratio also affects the amount of shear and normal stress concentration associated with a local discontinuity in material properties (Karimi and Barrat, 2018). The fact that the ~~fracture angle~~ LKF orientation is not affected by the changes in Poisson ratio thus indicates that the stress concentration and propagation of the fracture in space is mainly controlled by the stress correction rather than by the relaxation of material properties with damage. We speculate that the sensitivity of the ~~fracture angle~~ LKF orientation to the Poisson ratio in the standard stress correction scheme stems from the dependency of the stress correction path angle to the super-critical stress state (i.e. $\gamma = tan^{-1}(\sigma'_I/\sigma'_{II})$).

6 Discussion

The results presented above show that the generalized stress correction scheme reduces the growth of the residual error associated with the damage parameterization. Despite the improvement, some asymmetries are still present in the simulations ($\epsilon_{asym} < 10^{-2}$). This is due to the memory in the damage parameter (i.e. an integrated quantity) where residual errors accumulate and influence the temporal evolution of the solution. In regions of heavily damaged ice, the accumulated errors in the damage parameter result in large errors in the stress state due to the cubic dependence of the Maxwell viscosity η on d (Eq. 9). Future work includes replacing this formulation with a function that decreases the sensitivity of the Maxwell viscosity η for small changes in d around $d = 1$.

Overall, the use of a decohesive stress tensor yields smaller simulated ~~fracture~~ LKF angles, without significantly impacting the material deformations. Using a large correction path angle γ ($> 45°$), however, significantly slows the damage production and reduces the simulated sensitivity of the ~~fracture angle~~ LKF orientation to the mechanical strength parameters. Based on these results, we suggest using a correction path that is normal to the yield criterion ($\gamma = \arctan\mu$). This value brings the simulated ~~fracture~~ LKF angles closer to observations (see black points in Fig. 9) and reduces the amplification of residual errors, while correcting the super-critical stresses towards the closest point on the yield curve. Our implementation thus represents a generalization of the damage parameterization that can be easily implemented numerically and used to improve the performance of MEB models. Whether these improvements are also seen in the context of pan-Arctic simulations however remains to be tested, and is the subject of future work.

The simulation results show that in the MEB model, the damage develops at short time scales during which the elastic component of the rheology is important, while most of the deformations occur post-fracture over a longer time scale in the heavily damaged ice. This is in ~~stark~~ contrast with plastic models, in which a flow rule simultaneously dictates both the ~~fracture~~ LKF development and the relative amount of shear and normal deformations occurring ~~in the fractures~~along the LKFs. The

decoupling between the development of damage and the post-fracture deformations in the MEB model explains that the type of deformations in the ~~fracture~~ LKFs remains similar (uniaxial convergence, i.e. ridging, contrary to observation, Stern et al., 1995) despite the use of different stress correction path γ. This behaviour stems from the dominance of the viscous regime post-fracture: lead opening cannot occur when the stress state is compressive and remains limited to locations where tensile stresses are present, such as at the intersection of ~~lines of fracture~~the LKFs. This is contrary to granular theories, in which the distribution of contact normals determines the amount of ridging or lead opening (i.e. dilatancy) that is occurring when forced in uniaxial compression (Balendran and Nemat-Nasser, 1993). This indicates that the decohesive stress tensor cannot be used to influence the deformations associated to the fracture of ice in the MEB rheology unless other parameterizations, such as including a decohesive strain tensor during the fractures (e.g., see Schreyer et al., 2006; Sulsky and Peterson, 2011), are added to the rheology.

The viscous dissipation timescale (λ) in our model is set based on observations ($\sim 10^5$, Tabata, 1955; Hata and Tremblay, 2015), and is one order of magnitude smaller than in other MEB implementations (Dansereau et al., 2016; Rampal et al., 2019). The results from the model are robust with respect to the exact value of λ for a range $10^5 - 10^7$; the increase λ being compensated by larger damage values along the ~~fracture lines~~LKFs. For even larger λ values, ~~divergence~~ divergent deformations persist longer in the simulation and the transition from elastic- to viscous-dominated regime occurs later in the simulation (see Fig. 12), decreasing the overall convergence along the ~~fractures lines~~LKFs. If the transition to the viscous regime is removed (e.g. by setting $\alpha = 1$), divergence dominates throughout the simulations and ~~reach~~ reaches large values as the leads open. The elastic ~~wave are however~~waves, however, are no-longer dissipated in the ~~fractures~~LKFs, leading to large and noisy deformation fields (divergence/convergence). These findings call for a different viscosity-dependence on damage leading to both dissipation of elastic waves and a more realistic post-fracture deformation field.

Note that the results presented above ~~neglect heterogeneityin the ice cover, a factor that is responsible for much of the brittle material behaviour in progressive damage models (Amitrano and Helmstetter, 2006). Heterogeneity was neglected in the analysis above to isolate the growth of the residual errors. While including heterogeneities~~ were presented using a single space and time resolution, ice sample aspect ratio and without using heterogeneity. While the exact localisation of the LKFs in the simulations is affected by these parameters, the overall physics and sensitivity to the damage parameterization are robust to these changes. For instance, repeating the experiment by doubling the space resolution or the width of the ice sample does not change the ~~overall physics and sensitivity to the damage parameterization, it creates~~ LKF position and orientation (not shown). On the other hand, adding heterogeneity changes the LKF development by forming irregular sliding planes instead of the linear diamond ~~shape fractures~~ shapes (Fig. 13a), naturally creating contact points where ridging occurs with lead opening elsewhere along the ~~fracture lines. This results in~~ LKFs. This effectively creates a form of ~~granular~~ dilatancy typical of granular materials ~~.~~ (see alternating divergence and convergence in Fig. 13c) and leads to the formation of many secondary fractures, but the overall LKF orientations and their sensitivities otherwise remain the same as presented in this manuscript. Heterogeneity was however documented to be responsible for the localisation and intermittency of the sea-ice fractures, properties that are not investigated in our manuscript. These properties and their sensitivity to the decohesive stress tensor and other physical or numerical parameters requires more investigation and is the subject of future work.

7 conclusion

We propose a generalized stress correction scheme for the damage parameterization to reduce the growth of residual errors in the MEB sea ice model documented in (Plante et al., 2020). To this end, we scale the damage factor Ψ based on the super-critical maximum shear stress invariant (σ'_{II}) only, together with a decohesive stress tensor defining the path from the super-critical stress state to the yield curve. ~~The sensitivity of the fracture angles and~~ With this added flexibility to the choice of stress correction path, we determine the influence of the super-critical stress correction on the simulated sea-ice deformations ~~to these changes are investigated~~ and LKF orientation in the context of ~~the uniaxial compression experiment~~ uniaxial compression experiments similar to those presented in Ringeisen et al. (2019). This knowledge will serve as a basis for the development of other components to the damage parameterization to improve the simulated sea-ice deformations.

Our results show that in the MEB rheology, most of the deformations occur post-fracture in heavily damaged ice, where the viscous term is dominant. This causes a predominance of convergence (ridging) in the ~~fractures~~LKFs, contrary to laboratory experiments of granular materials and satellite observations of sea ice. The use of a decohesive stress tensor influences the ~~fracture angle of sea ice~~ LKF orientation in the sea ice cover, but does not influence the type of deformation rates (convergence and shear), nor the simulated dilatancy. Future work will involve the modification of the non-linear relationship between the Maxwell viscosity and the damage. We also show that the sensitivity of the ~~fracture angle~~ LKF orientation to the Poisson ratio, seen when using the standard damage parameterization, disappears when using the ~~generalizes~~ generalized stress correction scheme with a fixed stress correction path. This suggests that in the MEB model, the stress concentration and fracture propagation is governed by the stress correction rather than by the relaxation of the mechanical properties associated with the damage.

Based on our results, using the generalized damage parameterization with a stress correction path normal to the yield curve reduces the growth of residual errors and allows ~~for the production of~~ longer term simulations with post-fracture deformations. Using this stress correction path also reduces the ~~fracture angles~~ orientation of LKFs by $\sim 5°$, bringing them ~~in the range of~~ closer to observations. Despite these improvements, some error growth remains inherent to the formulation of the damage parameterization. Whether this might be improved by removing the dependency of the damage parameters on the damage factor (and on the super-critical stress state) will be explored in future work.

Code availability. Our sea-ice model code and outputs are available upon request.

Author contributions. M. Plante coded the model, ran all the simulations, analyzed results and led the writing of the manuscript. B. Tremblay participated in regular discussions during the course of the work and edited the manuscript.

Competing interests. The authors declare that they have no conflict of interest.

Acknowledgements. Our sea-ice model code and outputs are available upon request. Mathieu Plante would like to thank the Fonds de recherche du Québec – Nature et technologies (FRQNT) for financial support received during the course of this work. Bruno Tremblay is grateful for support from the Natural Science and Engineering and Research Council (NSERC) Discovery Program and the Office of Naval Research (N000141110977). This work is a contribution to the research program of Québec-Océan and of the ArcTrain International Training Program.

References

Aksenov, Y., Popova, E. E., Yool, A., Nurser, A. J. G., Williams, T. D., Bertino, L., and Bergh, J.: On the future navigability of Arctic sea routes : High-resolution projections of the Arctic Ocean and sea ice, Marine Policy, 75, 300–317, https://doi.org/10.1016/j.marpol.2015.12.027, http://dx.doi.org/10.1016/j.marpol.2015.12.027, 2017.

Amitrano, D. and Helmstetter, A.: Brittle creep, damage and time to failure in rocks, Journal of Geophysical Research : Solid Earth, 111, B11 201, https://doi.org/10.1029/2005JB004252, https://hal.archives-ouvertes.fr/hal-00172671, 2006.

Amitrano, D., Grasso, J.-R., and Hantz, D.: From diffuse to localised damage through elastic interaction, Geophysical Research Letters, 26, 2109–2112, 1999.

Arthur, J. R. F., Dunstan, T., Al-Ani, Q. A. J. L., and Assadi, A.: Plastic deformation and failure in granular media, Géotechnique, 27, 53–74, https://doi.org/10.1680/geot.1977.27.1.53, https://doi.org/10.1680/geot.1977.27.1.53, 1977.

Balendran, B. and Nemat-Nasser, S.: Double sliding model for cyclic deformation of granular materials, including dilatancy effects, Journal of the Mechanics and Physics of Solids, 41, 573–612, https://doi.org/https://doi.org/10.1016/0022-5096(93)90049-L, https://www.sciencedirect.com/science/article/pii/002250969390049L, 1993.

Bardet, J.: Orientation of shear bands in frictional soils, Journal of Engineering Mechanics - ASCE, 117, 1466–1484, https://doi.org/10.1061/(ASCE)0733-9399(1991)117:7(1466), 1991.

Bolton, M. D.: The strength and dilatancy of sands, Geotechnique, 36, 65–78, https://doi.org/10.1680/geot.1986.36.1.65, https://doi.org/10.1680/geot.1986.36.1.65, 1986.

Bouchat, A. and Tremblay, B.: Using sea-ice deformation fields to constrain the mechanical strength parameters of geophysical sea ice, Journal of Geophysical Research: Oceans, 122, 5802–5825, https://doi.org/10.1002/2017JC013020, https://agupubs.onlinelibrary.wiley.com/doi/abs/10.1002/2017JC013020, 2017.

Bouchat, A., Hutter, N. C., Chanut, J., Dupont, F., Dukhovskoy, D. S., Garric, G., Lee, Y. J., Lemieux, J.-F., Lique, C., Losch, M., and et al.: Sea Ice Rheology Experiment (SIREx), Part I: Scaling and statistical properties of sea-ice deformation fields, Earth and Space Science Open Archive, p. 36, https://doi.org/10.1002/essoar.10507397.1, https://doi.org/10.1002/essoar.10507397.1, 2021.

Bouillon, S. and Rampal, P.: Presentation of the dynamical core of neXtSIM, a new sea ice model, Ocean Modelling, 91, 23–37, https://doi.org/10.1016/j.ocemod.2015.04.005, http://dx.doi.org/10.1016/j.ocemod.2015.04.005, 2015.

Carrier, A., Got, J.-L., Peltier, A., Ferrazzini, V., Staudacher, T., Kowalski, P., and Boissier, P.: A damage model for volcanic edifices: Implications for edifice strength, magma pressure, and eruptive processes, Journal of Geophysical Research: Solid Earth, 120, 567–583, https://doi.org/10.1002/2014JB011485, https://agupubs.onlinelibrary.wiley.com/doi/abs/10.1002/2014JB011485, 2015.

Coon, M. D., Maykut, G. A., Pritchard, R. S., Rothrock, D. A., and Thorndike, A. S.: Modeling the pack ice as an elastic-plastic material, AIDJEX bulletin, 24, 1–105, https://doi.org/10.1017/CBO9781107415324.004, 1974.

Coulomb, C.: Test on the applications of the rules of maxima and minima to some problems of statics related to architecture, Mem Math Phys, 7, 343–382, 1773.

Damsgaard, A., Adcroft, A., and Sergienko, O.: Application of Discrete Element Methods to Approximate Sea Ice Dynamics, Journal of Advances in Modeling Earth Systems, 10, 2228–2244, https://doi.org/10.1029/2018MS001299, https://agupubs.onlinelibrary.wiley.com/doi/abs/10.1029/2018MS001299, 2018.

Dansereau, V., Weiss, J., Saramito, P., and Lattes, P.: A Maxwell elasto-brittle rheology for sea ice modelling, The Cryosphere, 10, 1339–1359, https://doi.org/10.5194/tc-10-1339-2016, https://tc.copernicus.org/articles/10/1339/2016/, 2016.

Dansereau, V., Weiss, J., Saramito, P., Lattes, P., and Coche, E.: Ice bridges and ridges in the Maxwell-EB sea ice rheology, The Cryosphere, 11, 2033–2058, https://doi.org/10.5194/tc-11-2033-2017, https://tc.copernicus.org/articles/11/2033/2017/, 2017.

Dansereau, V., Démery, V., Berthier, E., Weiss, J., and Ponson, L.: Collective Damage Growth Controls Fault Orientation in Quasibrittle Compressive Failure, Phys. Rev. Lett., 122, 085 501, https://doi.org/10.1103/PhysRevLett.122.085501, https://link.aps.org/doi/10.1103/PhysRevLett.122.085501, 2019.

Erlingsson, B.: Two-Dimensional Deformation Patterns in Sea Ice, Journal of Glaciology, 34, 301–308, https://doi.org/10.3189/S0022143000007061, 1988.

Girard, L., Bouillon, S., Weiss, J., Amitrano, D., Fichefet, T., and Legat, V.: A new modeling framework for sea-ice mechanics based on elasto-brittle rheology, Annals of Glaciology, 52, 123–132, https://doi.org/10.3189/172756411795931499, 2011.

Hata, Y. and Tremblay, L. B.: Anisotropic internal thermal stress in sea ice from the Canadian Arctic Archipelago, Journal of Geophysical Research: Oceans, 120, 5457–5472, https://doi.org/https://doi.org/10.1002/2015JC010819, https://agupubs.onlinelibrary.wiley.com/doi/abs/10.1002/2015JC010819, 2015.

Herman, A.: Discrete-Element bonded-particle Sea Ice model DESIgn, version 1.3a – model description and implementation, Geoscientific Model Development, 9, 1219–1241, https://doi.org/10.5194/gmd-9-1219-2016, https://gmd.copernicus.org/articles/9/1219/2016/, 2016.

Hibler, W. D.: A dynamic thermodynamic sea ice model, Journal of Physical Oceanography, 9, 815–846, 1979.

Hibler III, W. D. and Schulson, E. M.: On modeling the anisotropic failure and flow of flawed sea ice, Journal of Geophysical Research: Oceans, 105, 17 105–17 120, https://doi.org/10.1029/2000JC900045, https://agupubs.onlinelibrary.wiley.com/doi/abs/10.1029/2000JC900045, 2000.

Hunke, E. C.: Viscous–Plastic Sea Ice Dynamics with the EVP Model: Linearization Issues, Journal of Computational Physics, 170, 18 – 38, https://doi.org/https://doi.org/10.1006/jcph.2001.6710, http://www.sciencedirect.com/science/article/pii/S0021999101967105, 2001.

Hunke, E. C. and Dukowicz, J. K.: An Elastic–Viscous–Plastic Model for Sea Ice Dynamics, Journal of Physical Oceanography, 27, 1849 – 1867, https://doi.org/10.1175/1520-0485(1997)027<1849:AEVPMF>2.0.CO;2, https://journals.ametsoc.org/view/journals/phoc/27/9/1520-0485_1997_027_1849_aevpmf_2.0.co_2.xml, 1997.

Hutter, N. and Losch, M.: Feature-based comparison of sea ice deformation in lead-permitting sea ice simulations, The Cryosphere, 14, 93–113, https://doi.org/10.5194/tc-14-93-2020, https://tc.copernicus.org/articles/14/93/2020/, 2020.

Hutter, N., Losch, M., and Menemenlis, D.: Scaling Properties of Arctic Sea Ice Deformation in a High-Resolution Viscous-Plastic Sea Ice Model and in Satellite Observations, Journal of Geophysical Research: Oceans, 123, 672–687, https://doi.org/10.1002/2017JC013119, https://agupubs.onlinelibrary.wiley.com/doi/abs/10.1002/2017JC013119, 2018.

Hutter, N., Zampieri, L., and Losch, M.: Leads and ridges in Arctic sea ice from RGPS data and a new tracking algorithm, The Cryosphere, 13, 627–645, https://doi.org/10.5194/tc-13-627-2019, https://tc.copernicus.org/articles/13/627/2019/, 2019.

Hutter, N. C., Bouchat, A., Dupont, F., Dukhovskoy, D. S., Koldunov, N. V., Lee, Y. J., Lemieux, J.-F., Lique, C., Losch, M., Maslowski, W., and et al.: Sea Ice Rheology Experiment (SIREx), Part II: Evaluating simulated linear kinematic features in high-resolution sea-ice simulations, Earth and Space Science Open Archive, p. 35, https://doi.org/10.1002/essoar.10507396.1, https://doi.org/10.1002/essoar.10507396.1, 2021.

Itkin, P., Spreen, G., Hvidegaard, S. M., Skourup, H., Wilkinson, J., Gerland, S., and Granskog, M. A.: Contribution of Deformation to Sea Ice Mass Balance: A Case Study From an N-ICE2015 Storm, Geophysical Research Letters, 45, 789–796, https://doi.org/10.1002/2017GL076056, https://agupubs.onlinelibrary.wiley.com/doi/abs/10.1002/2017GL076056, 2018.

Jung, T., Gordon, N. D., Bauer, P., Bromwich, D. H., Chevallier, M., Day, J. J., Dawson, J., Doblas-Reyes, F., Fairall, C., Goessling, H. F., Holland, M., Inoue, J., Iversen, T., Klebe, S., Lemke, P., Losch, M., Makshtas, A., Mills, B., Nurmi, P., Perovich, D., Reid, P., Renfrew, I. A., Smith, G., Svensson, G., Tolstykh, M., and Yang, Q.: Advancing Polar Prediction Capabilities on Daily to Seasonal Time Scales, Bulletin of the American Meteorological Society, 97, 1631–1647, https://doi.org/10.1175/BAMS-D-14-00246.1, https://doi.org/10.1175/BAMS-D-14-00246.1, 2016.

Karimi, K. and Barrat, J.-L.: Correlation and shear bands in a plastically deformed granular medium, Scientific Reports, 8, 4021, https://doi.org/10.1038/s41598-018-22310-z, https://doi.org/10.1038/s41598-018-22310-z, 2018.

Kimmritz, M., Danilov, S., and Losch, M.: The adaptive EVP method for solving the sea ice momentum equation, Ocean Modelling, 101, 59 – 67, https://doi.org/https://doi.org/10.1016/j.ocemod.2016.03.004, http://www.sciencedirect.com/science/article/pii/S1463500316300038, 2016.

Koldunov, N. V., Danilov, S., Sidorenko, D., Hutter, N., Losch, M., Goessling, H., Rakowsky, N., Scholz, P., Sein, D., Wang, Q., and Jung, T.: Fast EVP Solutions in a High-Resolution Sea Ice Model, Journal of Advances in Modeling Earth Systems, 11, 1269–1284, https://doi.org/10.1029/2018MS001485, https://agupubs.onlinelibrary.wiley.com/doi/abs/10.1029/2018MS001485, 2019.

Kozo, T. L.: Initial model results for Arctic mixed layer circulation under a refreezing lead, Journal of Geophysical Research: Oceans, 88, 2926–2934, https://doi.org/10.1029/JC088iC05p02926, https://agupubs.onlinelibrary.wiley.com/doi/abs/10.1029/JC088iC05p02926, 1983.

Ledley, T. S.: A coupled energy balance climate-sea ice model: Impact of sea ice and leads on climate, Journal of Geophysical Research: Atmospheres, 93, 15 919–15 932, https://doi.org/10.1029/JD093iD12p15919, https://agupubs.onlinelibrary.wiley.com/doi/abs/10.1029/JD093iD12p15919, 1988.

Lemieux, J.-F., Tremblay, B., Thomas, S., Sedláček, J., and Mysak, L. A.: Using the preconditioned Generalized Minimum RESidual (GMRES) method to solve the sea-ice momentum equation, Journal of Geophysical Research: Oceans, 113, https://doi.org/https://doi.org/10.1029/2007JC004680, https://agupubs.onlinelibrary.wiley.com/doi/abs/10.1029/2007JC004680, 2008.

Lemieux, J.-F., Knoll, D. A., Losch, M., and Girard, C.: A second-order accurate in time IMplicit–EXplicit (IMEX) integration scheme for sea ice dynamics, Journal of Computational Physics, 263, 375–392, https://doi.org/https://doi.org/10.1016/j.jcp.2014.01.010, https://www.sciencedirect.com/science/article/pii/S002199911400031X, 2014.

Li, X., Krueger, S. K., Strong, C., Mace, G. G., and Benson, S.: Midwinter Arctic leads form and dissipate low clouds, Nature Communications, 11, 206, https://doi.org/10.1038/s41467-019-14074-5, https://doi.org/10.1038/s41467-019-14074-5, 2020.

Lüpkes, C., Vihma, T., Birnbaum, G., and Wacker, U.: Influence of leads in sea ice on the temperature of the atmospheric boundary layer during polar night, Geophysical Research Letters, 35, https://doi.org/10.1029/2007GL032461, https://agupubs.onlinelibrary.wiley.com/doi/abs/10.1029/2007GL032461, 2008.

Main, I. G.: A damage mechanics model for power-law creep and earthquake aftershock and foreshock sequences, Geophysical Journal International, 142, 151–161, https://doi.org/10.1046/j.1365-246x.2000.00136.x, https://doi.org/10.1046/j.1365-246x.2000.00136.x, 2000.

Marko, J. R. and Thomson, R. E.: Rectilinear leads and internal motions in the ice pack of the western Arctic Ocean, Journal of Geophysical Research (1896-1977), 82, 979–987, https://doi.org/10.1029/JC082i006p00979, https://agupubs.onlinelibrary.wiley.com/doi/abs/10.1029/JC082i006p00979, 1977.

Matsumura, Y. and Hasumi, H.: Brine-Driven Eddies under Sea Ice Leads and Their Impact on the Arctic Ocean Mixed Layer, Journal of Physical Oceanography, 38, 146–163, https://doi.org/10.1175/2007JPO3620.1, https://doi.org/10.1175/2007JPO3620.1, 2008.

Maykut, G. A.: Large-scale heat exchange and ice production in the central Arctic, Journal of Geophysical Research: Oceans, 87, 7971–7984, https://doi.org/10.1029/JC087iC10p07971, https://agupubs.onlinelibrary.wiley.com/doi/abs/10.1029/JC087iC10p07971, 1982.

Mohr, O.: Welche Umstände bedingen die Elastizitätsgrenze und den Bruch eines Materials, Zeitschrift des Vereins Deutscher Ingenieure, 46, 1572–1577, 1900.

Murakami, S.: Continuum damage mechanics : a continuum mechanics approach to the analysis of damage and fracture, https://doi.org/10.1007/978-94-007-2666-6, http://site.ebrary.com/id/10537681, 2012.

Overland, J. E., McNutt, S. L., Salo, S., Groves, J., and Li, S.: Arctic sea ice as a granular plastic, Journal of Geophysical Research: Oceans, 103, 21 845–21 867, https://doi.org/https://doi.org/10.1029/98JC01263, https://agupubs.onlinelibrary.wiley.com/doi/abs/10.1029/98JC01263, 1998.

Plante, M., Tremblay, B., Losch, M., and Lemieux, J.-F.: Landfast sea ice material properties derived from ice bridge simulations using the Maxwell elasto-brittle rheology, The Cryosphere, 14, 2137–2157, https://doi.org/10.5194/tc-14-2137-2020, https://tc.copernicus.org/articles/14/2137/2020/, 2020.

Rampal, P., Bouillon, S., Ólason, E., and Morlighem, M.: neXtSIM: a new Lagrangian sea ice model, The Cryosphere, 10, 1055–1073, https://doi.org/10.5194/tc-10-1055-2016, https://www.the-cryosphere.net/10/1055/2016/, 2016.

Rampal, P., Dansereau, V., Olason, E., Bouillon, S., Williams, T., and Samaké, A.: On the multi-fractal scaling properties of sea ice deformation, The Cryosphere Discussions, 2019, 1–45, https://doi.org/10.5194/tc-2018-290, https://www.the-cryosphere-discuss.net/tc-2018-290/, 2019.

Rice, J. R.: Solid Mechanics, Harvard University 2010, 2010.

Ringeisen, D., Losch, M., Tremblay, L. B., and Hutter, N.: Simulating intersection angles between conjugate faults in sea ice with different viscous–plastic rheologies, The Cryosphere, 13, 1167–1186, https://doi.org/10.5194/tc-13-1167-2019, https://www.the-cryosphere.net/13/1167/2019/, 2019.

Ringeisen, D., Tremblay, L. B., and Losch, M.: Non-normal flow rules affect fracture angles in sea ice viscous–plastic rheologies, The Cryosphere, 15, 2873–2888, https://doi.org/10.5194/tc-15-2873-2021, https://tc.copernicus.org/articles/15/2873/2021/, 2021.

Roscoe, K. H.: The Influence of Strains in Soil Mechanics, Géotechnique, 20, 129–170, https://doi.org/10.1680/geot.1970.20.2.129, https://doi.org/10.1680/geot.1970.20.2.129, 1970.

Schreyer, H. L., Sulsky, D. L., Munday, L. B., Coon, M. D., and Kwok, R.: Elastic-decohesive constitutive model for sea ice, Journal of Geophysical Research: Oceans, 111, https://doi.org/https://doi.org/10.1029/2005JC003334, https://agupubs.onlinelibrary.wiley.com/doi/abs/10.1029/2005JC003334, 2006.

Schulson, E. M.: Compressive shear faults within arctic sea ice: Fracture on scales large and small, Journal of Geophysical Research: Oceans, 109, https://doi.org/10.1029/2003JC002108, https://agupubs.onlinelibrary.wiley.com/doi/abs/10.1029/2003JC002108, 2004.

Sodhi, D. S.: Ice arching and the drift of pack ice through restricted channels, Cold Regions Research and Engineering Laboratory (CRREL) Rep. 77-18, p. 11 pp., 1997.

Stern, H. L., Rothrock, D. A., and Kwok, R.: Open water production in Arctic sea ice: Satellite measurements and model parameterizations, Journal of Geophysical Research: Oceans, 100, 20 601–20 612, https://doi.org/10.1029/95JC02306, https://agupubs.onlinelibrary.wiley.com/doi/abs/10.1029/95JC02306, 1995.

Sulsky, D. and Peterson, K.: Toward a new elastic–decohesive model of Arctic sea ice, Physica D: Nonlinear Phenomena, 240, 1674–1683, https://doi.org/https://doi.org/10.1016/j.physd.2011.07.005, https://www.sciencedirect.com/science/article/pii/S0167278911001916, special Issue: Fluid Dynamics: From Theory to Experiment, 2011.

Tabata, T.: A Measurement of Visco-Elastic Constants of Sea Ice, Journal of the Oceanographical Society of Japan, 11, 185–189, 1955.

Timco, G. and Weeks, W.: A review of the engineering properties of sea ice, Cold Regions Science and Technology, 60, 107–129, https://doi.org/https://doi.org/10.1016/j.coldregions.2009.10.003, https://www.sciencedirect.com/science/article/pii/S0165232X09001797, 2010.

Tremblay, L.-B. and Hakakian, M.: Estimating the Sea Ice Compressive Strength from Satellite-Derived Sea Ice Drift and NCEP Reanalysis Data, Journal of Physical Oceanography, 36, 2165 – 2172, https://doi.org/10.1175/JPO2954.1, https://journals.ametsoc.org/view/journals/phoc/36/11/jpo2954.1.xml, 2006.

Tremblay, L.-B. and Mysak, L. A.: Modeling Sea Ice as a Granular Material, Including the Dilatancy Effect, Journal of Physical Oceanography, 27, 2342 – 2360, https://doi.org/10.1175/1520-0485(1997)027<2342:MSIAAG>2.0.CO;2, https://journals.ametsoc.org/view/journals/phoc/27/11/1520-0485_1997_027_2342_msiaag_2.0.co_2.xml, 1997.

Tuhkuri, J. and Lensu, M.: Laboratory tests on ridging and rafting of ice sheets, Journal of Geophysical Research: Oceans, 107, 8–1–8–14, https://doi.org/https://doi.org/10.1029/2001JC000848, https://agupubs.onlinelibrary.wiley.com/doi/abs/10.1029/2001JC000848, 2002.

Turnbull, I. D., Torbati, R. Z., and Taylor, R. S.: Relative influences of the metocean forcings on the drifting ice pack and estimation of internal ice stress gradients in the Labrador Sea, Journal of Geophysical Research: Oceans, 122, 5970–5997, https://doi.org/10.1002/2017JC012805, https://agupubs.onlinelibrary.wiley.com/doi/abs/10.1002/2017JC012805, 2017.

Vardoulakis, I.: Shear band inclination and shear modulus of sand in biaxial tests, International Journal for Numerical and Analytical Methods in Geomechanics, 4, 103–119, https://doi.org/10.1002/nag.1610040202, https://onlinelibrary.wiley.com/doi/abs/10.1002/nag.1610040202, 1980.

Wachter, L., Renshaw, C., and Schulson, E.: Transition in brittle failure mode in ice under low confinement, Acta Materialia, 57, 345–355, https://doi.org/https://doi.org/10.1016/j.actamat.2008.09.021, https://www.sciencedirect.com/science/article/pii/S1359645408006605, 2009.

Wang, K.: Observing the yield curve of compacted pack ice, Journal of Geophysical Research: Oceans, 112, https://doi.org/10.1029/2006JC003610, https://agupubs.onlinelibrary.wiley.com/doi/abs/10.1029/2006JC003610, 2007.

Wilchinsky, A. V. and Feltham, D. L.: A continuum anisotropic model of sea-ice dynamics, Proceedings of the Royal Society of London. Series A: Mathematical, Physical and Engineering Sciences, 460, 2105–2140, https://doi.org/10.1098/rspa.2004.1282, https://royalsocietypublishing.org/doi/abs/10.1098/rspa.2004.1282, 2004.

Wilchinsky, A. V., Heorton, H. D. B. S., Feltham, D. L., and Holland, P. R.: Study of the Impact of Ice Formation in Leads upon the Sea Ice Pack Mass Balance Using a New Frazil and Grease Ice Parameterization, Journal of Physical Oceanography, 45, 2025–2047, https://doi.org/10.1175/JPO-D-14-0184.1, https://doi.org/10.1175/JPO-D-14-0184.1, 2015.

Table 1. Default Model Parameters

Parameter	Definition	Value
Δx	Spatial resolution	1 km
Δt	Time step	0.2 s
T_d	Damage time scale	1 s
Y	Young Modulus	10^9 n m^{-2}
ν	Poisson ratio	0.33
λ_0	Viscous relaxation time	10^5 s
α	Viscous transition parameter	3
ϕ	Angle of internal friction	45°
c_0	Cohesion	10 N m^{-2}
σ_{c_0}	Isotropic compressive strength	50N m^{-2}
ρ_a	Air density	1.3 kg m^{-3}
ρ_i	Sea ice density	9.0×10^2 kg m^{-3}
ρ_w	Sea water density	1.026×10^3 kg m^{-3}
C_{da}	Air drag coefficient	1.2×10^{-3}
C_{dw}	Water drag coefficient	5.5×10^{-3}

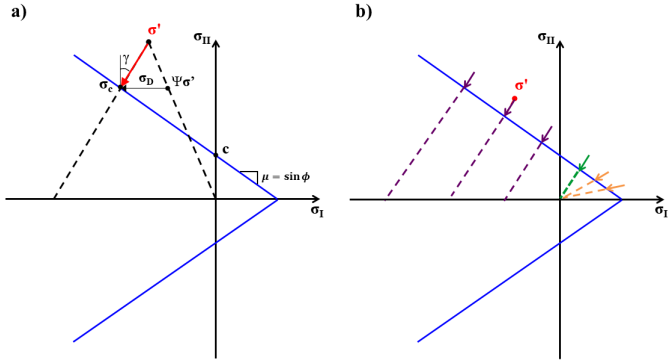

Figure 1. a) Mohr-Coulomb yield criterion ($\pm\sigma_{II} + \mu\sigma_I = c$, blue lines) in stress invariant space. $\boldsymbol{\sigma}'$ is the uncorrected super-critical stress state, $\boldsymbol{\sigma}_c$ the critical stress state for a given correction path angle γ (red dashed line) and c is the cohesion. The decohesive stress tensor $\boldsymbol{\sigma}_D$ is defined as the difference between $\boldsymbol{\sigma}_c$ and the scaled super-critical stress ($\Psi\boldsymbol{\sigma}'$). b) Proposed correction paths for various super-critical stresses $\boldsymbol{\sigma}'$ that minimizes the error amplification ratio (R), which consist of the standard parameterization for large tensile stresses (orange) and a correction path with γ = 45° for small tensile and compressive stresses (purple). The green line indicates the transition between the two formulations.

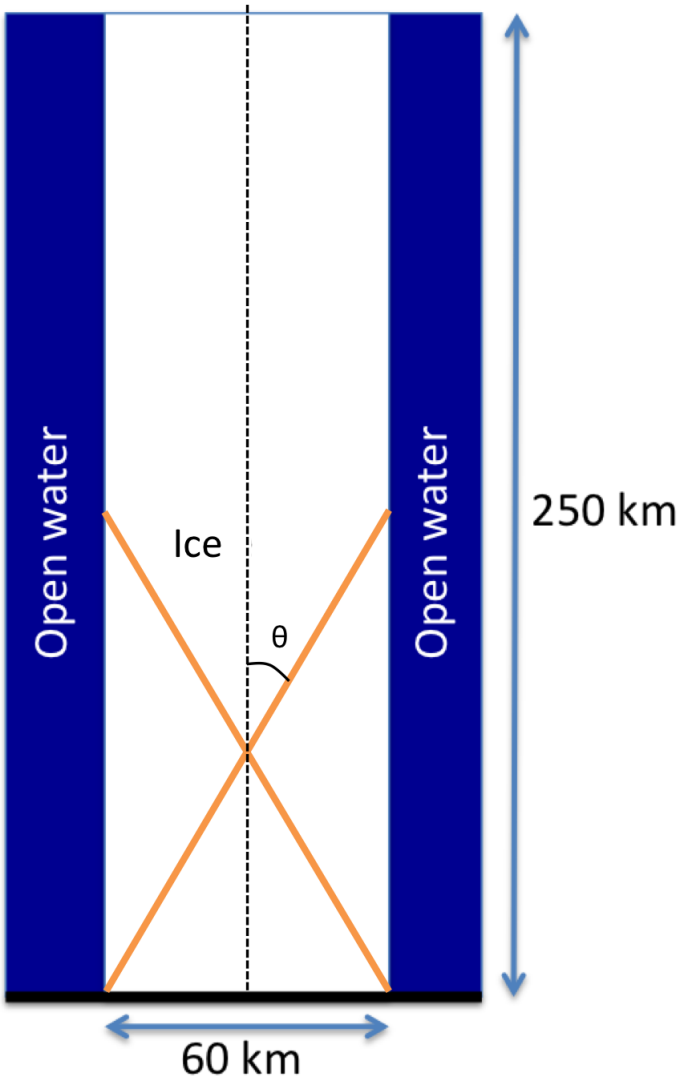

Figure 2. Idealized domain for uniaxial compression simulations, with a solid boundary (Dirichlet conditions, $u = v = 0$) at the bottom, and open boundaries (Neumann conditions, $\partial u/\partial n = 0$) on the sides and top. The initial conditions are h = 1m and A = 100% in a region of 250 x 60 km in the center of the domain (white), with two 20 km wide bands of open water on each side (blue). The ~~fracture angle~~ orientation of the LKFs (θ) is defined as half of the angle between conjugate pairs of fracture lines (~~Orange~~ orange lines).

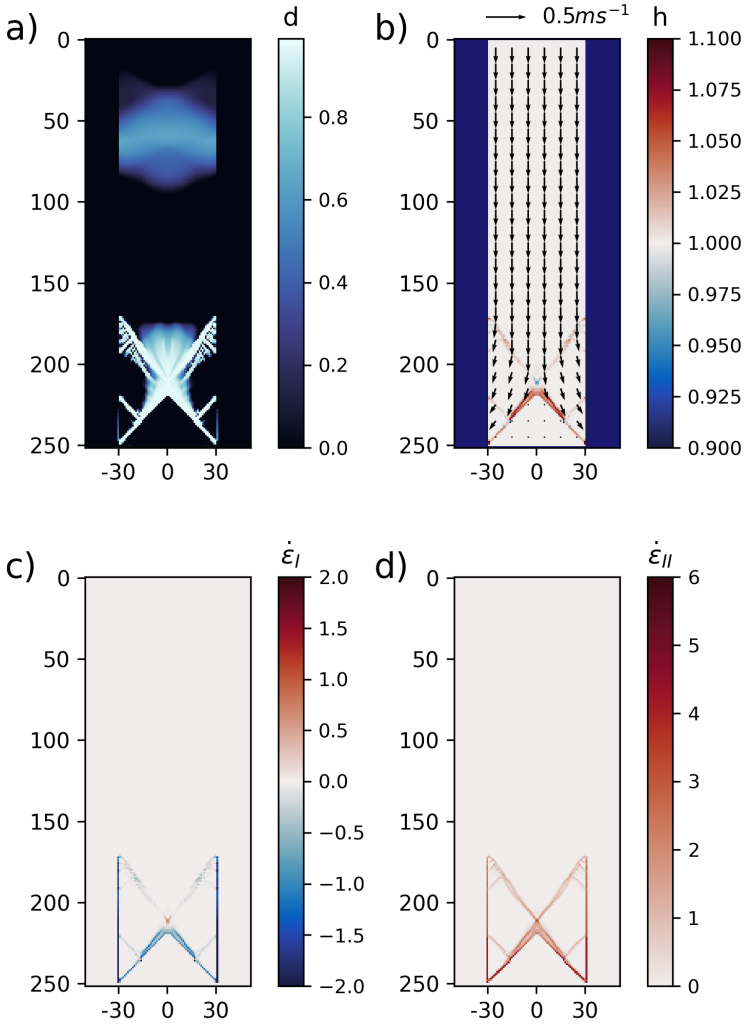

Figure 3. a) Damage (unitless), b) ice thickness (m, color) and velocity vectors (m s^{-1}), c) mean normal strain rate invariant ($\dot{\epsilon}_I$, day^{-1}) and d) ~~mixiumum~~ maximum shear strain rate invariant ($\dot{\epsilon}_{II}$, $days^{-1}$), after two hours of integration in the control simulation using the standard stress correction scheme.

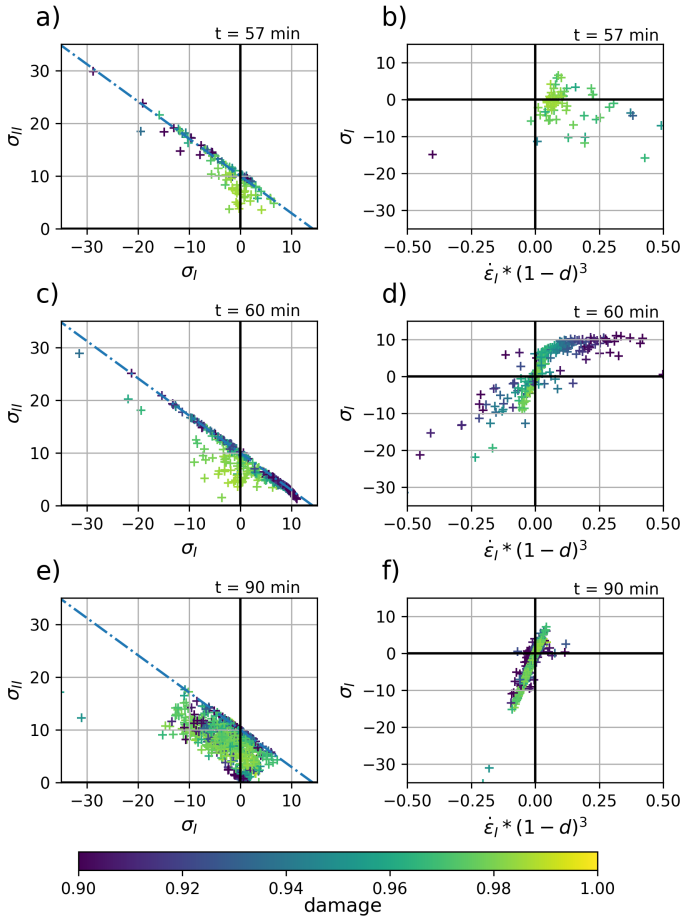

Figure 4. ~~Stress~~ Scatter plots of local stress invariants (σ_I vs. σ_{II}, in kN m^{-1}, left column) ~~and~~ , normal stresses and scaled strain rate ~~invariant scaled by the $(1-d)^3$~~ invariants (~~day^{-1}x10^3) as a function of the normal stress invariant (kN m^{-1}~~ σ_I vs. $(1-d)^3\dot{\epsilon}_{II}$, right column) ~~,~~ in ~~the control simulation for~~ heavily damaged (d > 0.9) grid cells, at t = ~~60~~ 57 min (during the fracture development, top row), t = ~~120~~ 60 min (a few minutes after the fracture, middle row), and t = ~~180~~ 90 min (~ 30 min after the fracture, bottom row). Color indicates the local damage. The strain rates are normalised to account for the non-linear dependency of the viscosity η on the damage parameter. The gradual alignment of the points in the σ_I vs. $(1-d)^3\dot{\epsilon}_{II}$ diagram indicate the development of a linear-viscous stress-strain relationship over time.

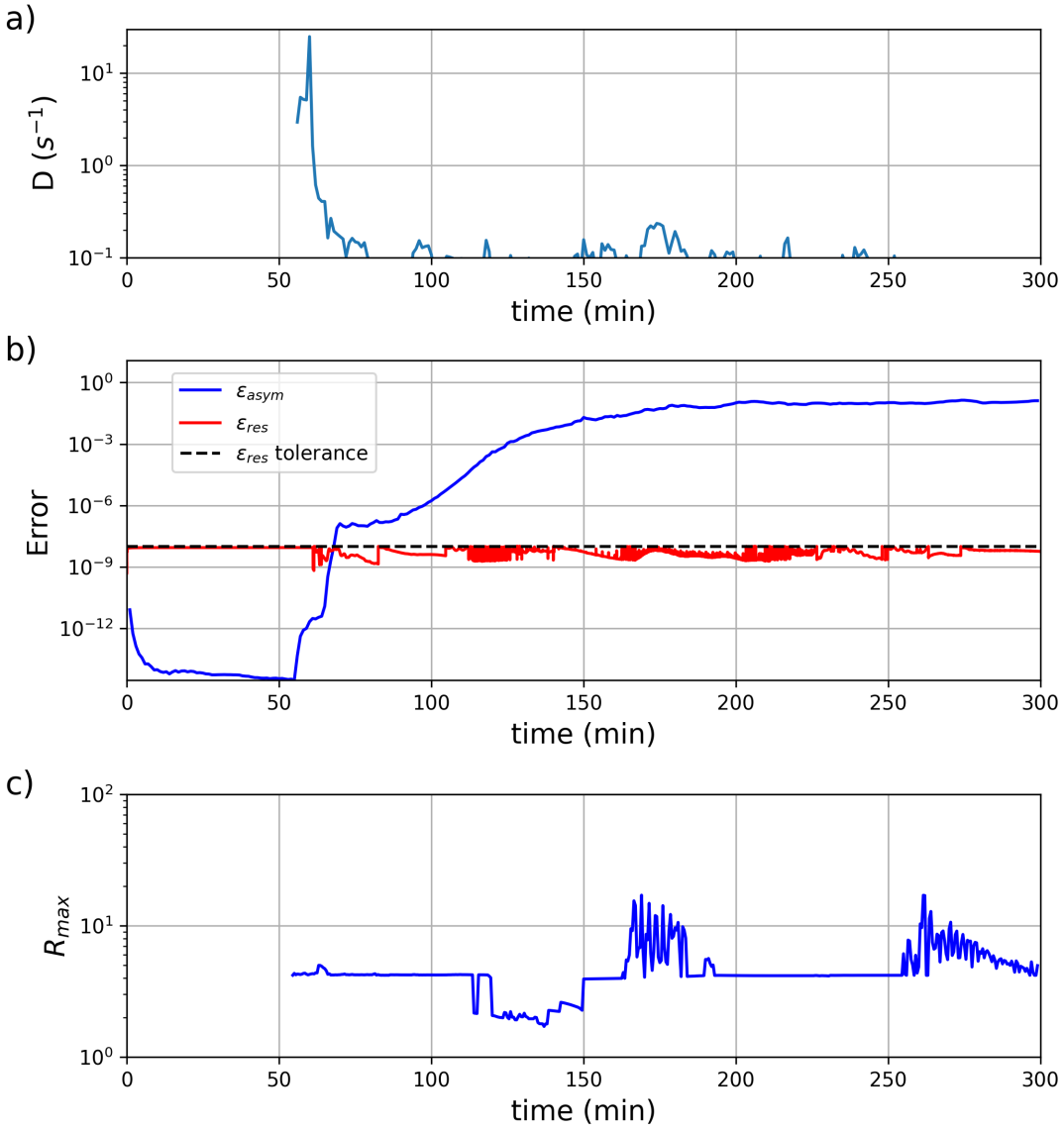

Figure 5. a) Temporal evolution of the damage activity D, b) the solution residual ϵ_{res}, asymmetry factor ϵ_{asym} and convergence criterion on ϵ_{res}, and c) the maximum error amplification ratio R_{max}, in the control simulation using the standard stress correction scheme.

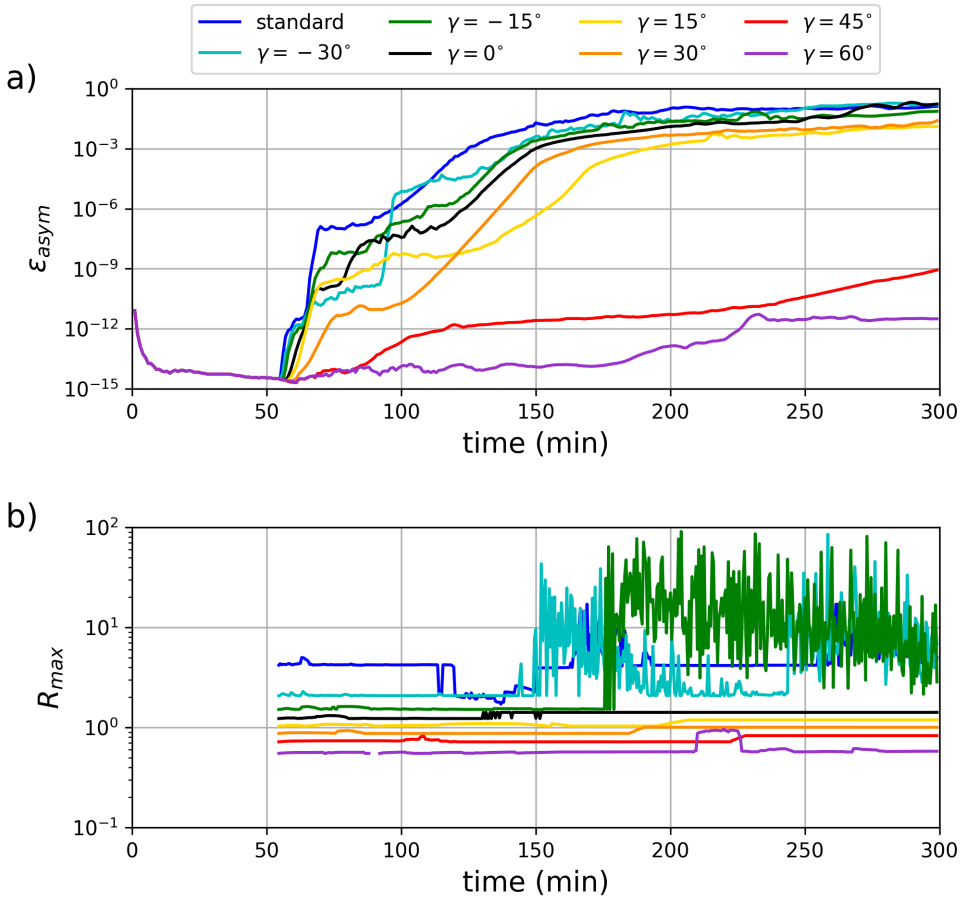

Figure 6. a) ~~Temporal~~ Time evolution of the asymmetry factor ϵ_{asym} and b) time series of the maximum error amplification ratio R_{max} ~~and b) the asymmetry factor ϵ_{asym}~~, in a sensitivity experiment on the stress correction path angle γ, using the generalized stress correction scheme.

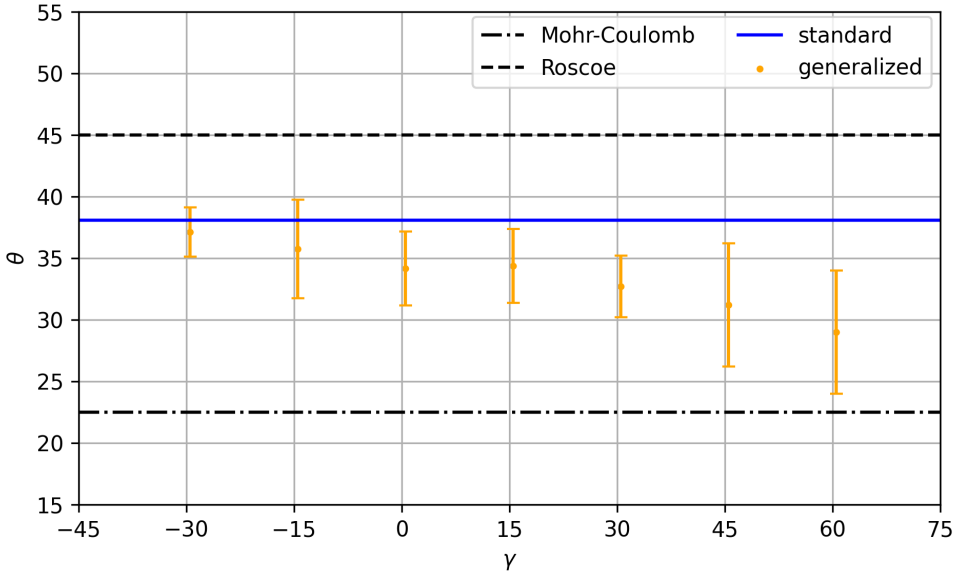

Figure 7. Sensitivity of the ~~fracture angle~~ LKF orientation θ on the stress correction path angle γ (degrees) in uniaxial loading experiments using the generalized stress correction schemes. The theoretical LKF angles from the Mohr-Coulomb and Roscoe theories are indicated by dash-dotted and dashed lines respectively for reference.

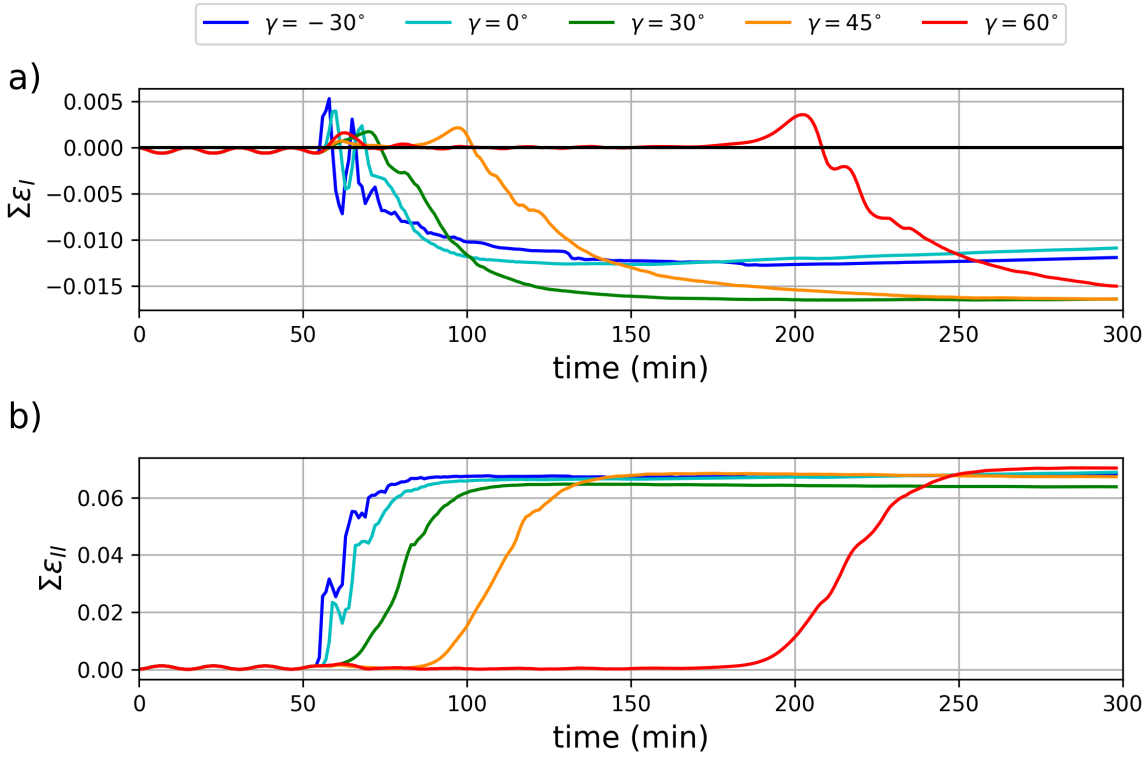

Figure 8. Time evolution of the mean normal (a) and maximum shear (b) strain rate invariants integrated over the ice cover, in simulations using the generalized damage parameterization with different stress correction path γ.

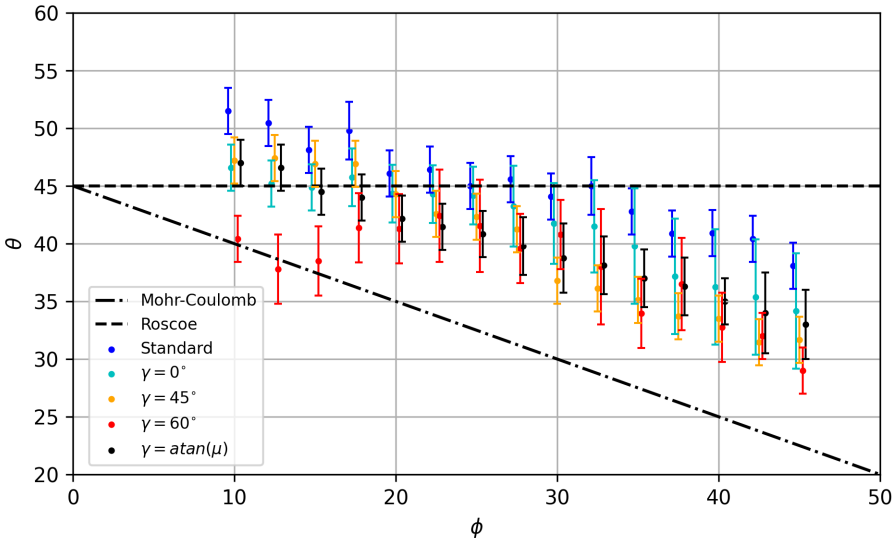

Figure 9. Sensitivity of the ~~fracture angles~~ LKF orientation (θ, degrees) on the angle of internal friction (ϕ, degrees), in uniaxial loading experiments using different correction path angle (γ). The correction path angle $\gamma = atan(\mu)$ implies that the stress correction path is perpendicular to the yield curve. The theoretical ~~fracture angle~~ LKF orientation from the Mohr-Coulomb and Roscoe theories are indicated by ~~dashed and~~ dash-dotted and dashed lines respectivelty for reference.

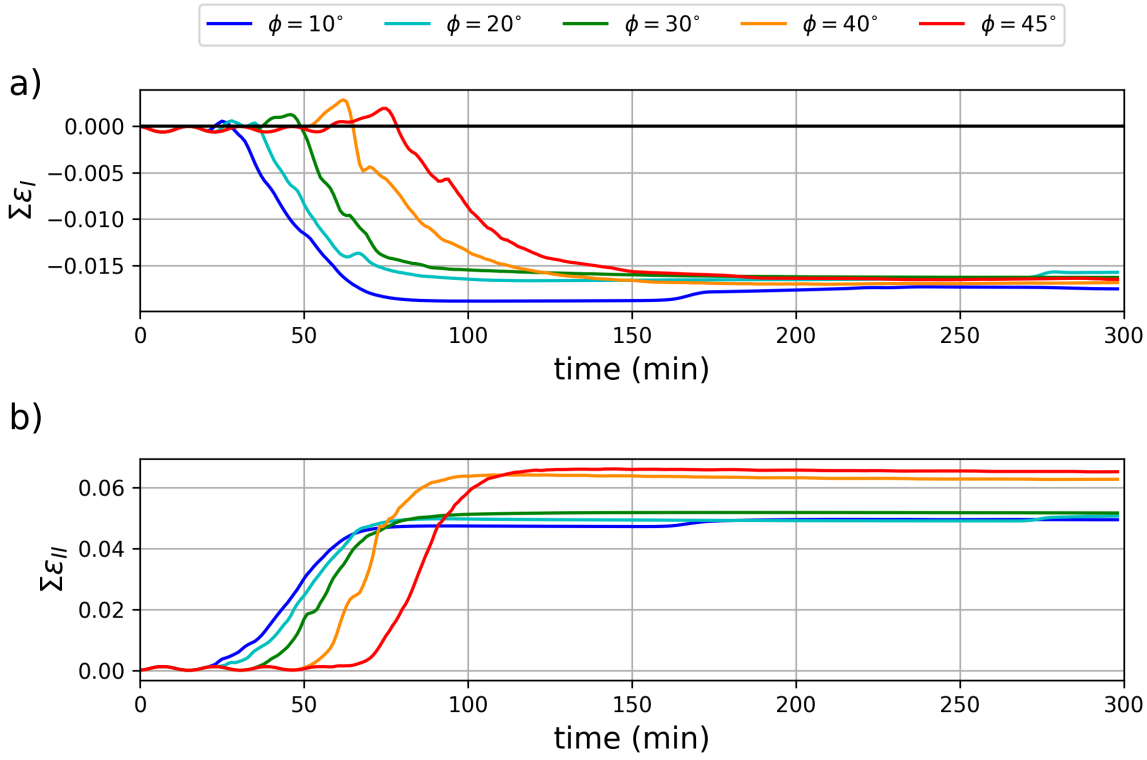

Figure 10. Time evolution of a) the mean normal strain rate invariant integrated over the ice cover (day^{-1}) and b) the maximum shear strain rate invariant integrated over the ice cover (day^{-1}), when using different angles of internal friction ϕ, with a stress correction path normal to the yield curve ($\gamma = \arctan(\mu)$).

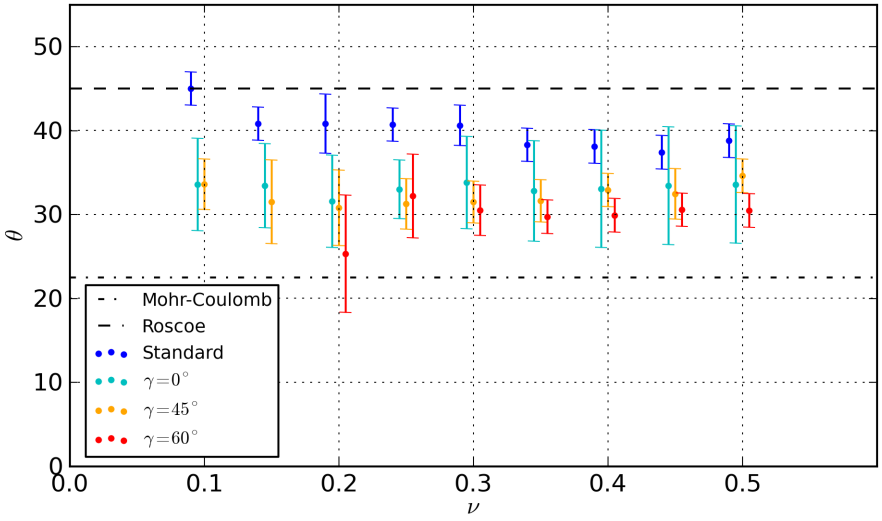

Figure 11. Sensitivity of the ~~fracture angles~~ LKF orientation (θ, degrees) on the Poisson ratio (ν, unitless), in uniaxial loading experiments using different correction path angle (γ). The theoretical ~~fracture angle~~ orientations from the Mohr-Coulomb and Roscoe theories are indicated by ~~dashed and~~ dash-dotted and dashed lines respectively for reference.

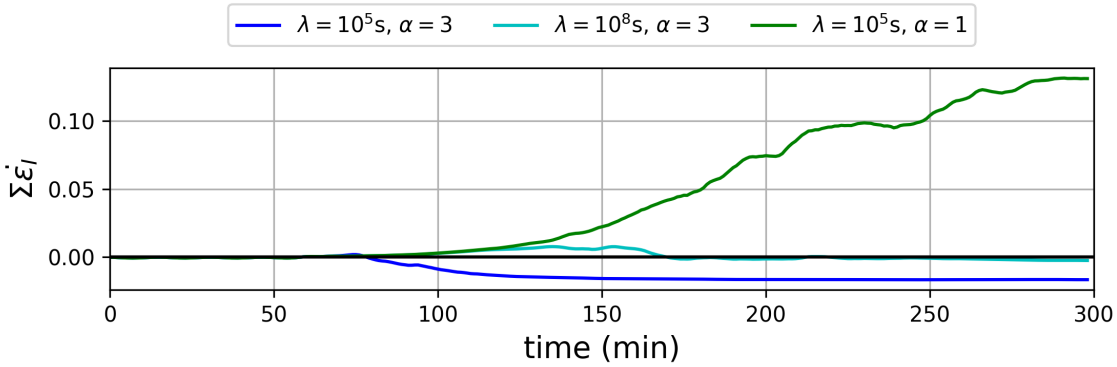

Figure 12. Time evolution of the mean normal strain rate invariant integrated over the ice cover (day^{-1}) using a stress correction path normal to the yield curve ($\gamma = \arctan(\mu)$) with $\alpha = 3$ (blue), $\alpha = 1$, and a longer viscous dissipation time-scale ($\lambda = 10^8$ s).

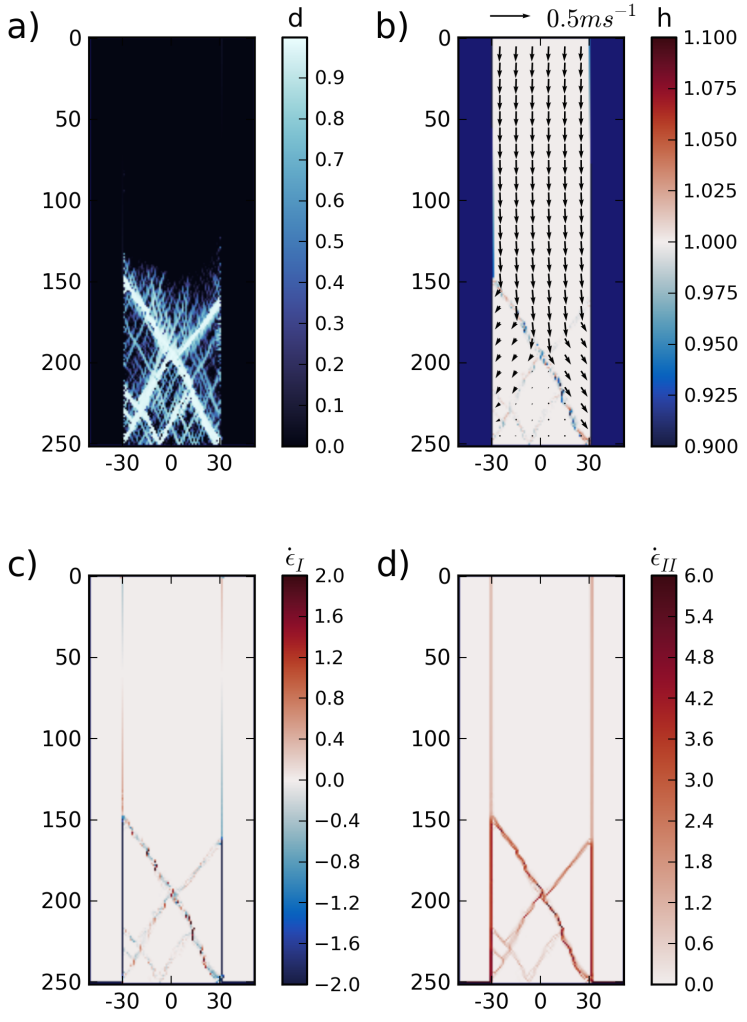

Figure 13. a) Damage (unitless), b) ice thickness (m, color) and velocity vectors (m s^{-1}), c) mean normal strain rate invariant ($\dot{\epsilon}_I$, day^{-1}) and d) maximum shear strain rate invariant ($\dot{\epsilon}_{II}$, $days^{-1}$) after two hours of integration in using the generalized stress correction scheme with $\gamma = 45^{\circ}$ and including heterogeneity in the initial material cohesion field. The heterogeneous cohesion (c_0) field is defined locally at each grid cell by picking a random number between 7.0 and 13.0 kN m^{-2}. The remaining initial conditions are the same as all other simulations.